

**Workshop on  
DUST ON MARS III**

---

**September 21 - 23, 1988**

---

**Sponsored by**

**THE LUNAR AND PLANETARY INSTITUTE**

**&**

**NATIONAL AERONAUTICS AND SPACE ADMINISTRATION (NASA)**

**ABSTRACTS PRESENTED TO THE MECA - LPI WORKSHOP:**

**Dust on Mars III**

Estes Park, Colorado  
September 21 - 23, 1988

Sponsored by

Lunar and Planetary Institute  
National Aeronautics and Space Administration (NASA)

Compiled in 1988

by

Lunar and Planetary Institute

Material in this volume may be copied without restraint for library, abstract service, educational, or personal research purposes; however, republication of any paper or portion thereof requires the written permission of the authors as well as appropriate acknowledgment of this publication.

## PREFACE

This volume contains abstracts that have been accepted for presentation at the MECA - LPI Workshop on Dust on Mars III. The Program Committee consisted of S. Lee, Workshop Organizer; B. Jakosky, R. Zurek; and P. Christensen.

Logistics and administrative support were provided by the Projects Office at the Lunar and Planetary Institute. This abstract volume was prepared by the Publications Office staff at the Lunar and Planetary Institute.

The Lunar and Planetary Institute is operated by the Universities Space Research Association under contract No. NASW-4066 with the National Aeronautics and Space Administration.

The subject of this report is the...

The purpose of this report is to...

The results of the study are...

The conclusions of the study are...

The recommendations of the study are...

The limitations of the study are...

The significance of the study is...

The scope of the study is...

The methodology of the study is...

The data of the study are...

The analysis of the data is...

The interpretation of the data is...

The summary of the study is...

The final conclusion of the study is...

## TABLE OF CONTENTS

<i>The Mineral Components of Dust on Mars</i> A. Banin .....	1
<i>Baroclinic-Radiative Instability and Martian Summer Polar Cyclones</i> J. R. Barnes .....	4
<i>Mars Observer Vims and Phobos KRFM-ISM Observations of Mars Dust</i> L. W. Esposito.....	6
<i>An Assessment of the Meteoric and Meteoritic Contributions to Dust on Mars</i> G. J. Flynn and D. S. McKay.....	7
<i>Possible Intense Vortices and the Potential for Dust and Sand Transport on Mars</i> J. A. Grant and P. H. Schultz.....	10
<i>Comparison of Martian Aeolian Features and Results from the Global Circulation Model</i> R. Greeley, A. Skyeck, and J. B. Pollack .....	13
<i>Simulations of the Martian Boundary Layer: Factors Controlling the Behavior of the Surface Stress</i> R. M. Haberle, J. B. Pollack, and J. Schaeffer .....	16
<i>The North Polar Sand Seas: Preliminary Estimates of Sediment Volume</i> N. Lancaster and R. Greeley.....	18
<i>Viking Photometric and Albedo Studies of Regional Dust Transport on Mars</i> S. W. Lee and R. T. Clancy .....	21
<i>Correlations Between Surface Albedo Features and Global Duststorms on Mars</i> L. J. Martin and P. B. James.....	23
<i>Earthbased Monitoring of the Martian Atmosphere Dust Opacity</i> T. Z. Martin.....	25
<i>Numerical Simulations of Global Dust Storm Decay</i> J. Murphy, O. B. Toon, J. B. Pollack, and R. M. Haberle .....	28
<i>Simulations of the General Circulation of the Martian Atmosphere II. Dust Storms</i> J. B. Pollack, R. M. Haberle, and J. Schaeffer .....	31
<i>Infrared Transmission Measurements of Martian Soil Analogs</i> T. L. Roush.....	32
<i>Dust in the Polar Regions of Mars: Is it the Same as at Low Latitudes?</i> P. C. Thomas.....	35
<i>Depolarized Radar Echoes and Dust on Mars</i> T. W. Thompson and H. J. Moore .....	36

<b><i>Mars Global Atmospheric Oscillations: Annually Synchronized, Transient Normal Mode Oscillations and the Triggering of Global Dust Storms</i></b> J. E. Tillman .....	39
<b><i>Martian Great Dust Storms: Aperiodic Phenomena?</i></b> R. W. Zurek and R. M. Haberle .....	40

THE MINERAL COMPONENTS OF DUST ON MARS; A. Banin, Dept. of Soil and Water Sciences, Hebrew University, 76100 Rehovot, Israel.

The mineral components of the dust on Mars have not yet been directly analyzed. Up to the present, the major source of information on dust components is the various analyses, both in situ and by remote sensing, of the Martian soil, i.e. the fine, weathered, loosely packed aeolian material covering major areas of the planet. Evidence shows that this soil material has been thoroughly homogenized by the global dust storms characteristic of Mars, and it is plausible to assume that Mars dust composition is strongly correlated with the top-soil composition. This compositional similarity may be strengthened on Mars, where conditions over the last geological epochs did not favor rapid alteration and weathering of minerals either in the soil or in the dust. Various approaches have been used to constrain the mineralogical composition of Mars soil. These were based on chemical correspondence with the analyses of the soil done by the Viking Landers, simulation of the spectral-remote sensing observations of Mars, simulations of Viking Biology and other Viking Lander experiments, and various modelling efforts. On the basis of these studies, the following candidates have been suggested:

1) Aluminosilicates: Smectite clays such as montmorillonite and the iron-rich nontronite have been initially suggested as best satisfying spectral (1,2) and chemical (3,4) properties. Further strong support was obtained from simulations of the Viking Biology experiments(5-8) and the modelling of the weathering processes on Mars(9,10). Smectites do not however show the magnetic susceptibility measured on Mars. Palagonite, a poorly defined weathering product of basalts, is another candidate which satisfies spectral and compositional constraints(11-13). It fails, however, in the simulation of the reactivity shown in the Viking Biology experiments(14,15).

2) Iron Minerals: Iron is a major chemical components in the Martian soil(3,4). Its minerals strongly affect the spectral characteristics of the soil in the visible range, lending the soil its characteristic reddish coloration. Reflectance spectra of the "bright" regions of Mars, believed to contain the more weathered components of the soil, show an intense though relatively featureless absorption edge from 0.75 $\mu$ m to the near ultraviolet(16,17). Several mineral candidates have been shown to satisfy these spectral constraints including "amorphous" iron oxides(18,19), palagonite(12), corundum doped with iron(20), jarosite(21), cryptocrystalline hematite deposited in silica matrix(22) and iron enriched smectites(7,8). The major conclusion from the abundance of spectral analogs is that unambiguous identification of the iron mineral(s) in Mars soil, on the basis of reflectance only, is not possible at present. The spectral evidence does show, however, that iron in the weathered component of Mars soil is mostly present in the oxidized form either in poorly crystallized clusters of oxy-hydroxy ferric iron, or as crystalline minerals, but in extremely small particle size range ("nanocrystals").

Smectite clays chemically enriched with ferrous iron, which is then oxidized and polymerized in situ(23), show strong spectral analogy with Mars (Fig. 1). Compositionally, these preparations are full chemical analogs of the Mars soil with respect to iron oxide content. X-ray diffractometry, chemical extractions and electron micrographs show that iron in these preparations is in poorly crystalline or cryptocrystalline compound(s) and appears in particles of size range 1-10 nm(24). In these Mars soil analogs the

Banin, A.

crystallization of iron oxide minerals and the growth of their crystals is apparently prevented (a) by the presence of Si and Al in the equilibrium solution, known to affect Fe oxide crystallization in soil environments(25), (b) by the presence of an adsorbing surface of the smectite which immobilizes colloidal iron-oxyhydroxy particles and reduces iron concentration in solution, thus slowing down or preventing the precipitation and crystallization of pure iron minerals. Similar conditions can prevail in Mars soil, explaining its spectral properties and chemical reactivity.

3) Carbonates: Although no spectral evidence for carbonates has been found yet on Mars (26) considerations of Mars climate evolution has led to suggestions that carbonate minerals should have been deposited on Mars(27) and shall, therefore, be present in the soil and dust on Mars. Recent simulations of the Viking Biology LR experiments using mixtures of the active ingredient (iron enriched smectite clays) with various carbonate minerals (Fig. 2) have shown that even low amounts (0.5-1.0%) of added calcite reduce considerably the decomposition activity of the smectite and diminish the release of  $^{14}\text{CO}_2$ , making the mixture an unlikely candidate for Mars soil. A much higher content of siderite ( $\text{FeCO}_3$ ) can be tolerated. Thus it is possible that the carbonate component, if present in Mars soil, may be siderite rather than calcite, magnesite or dolomite.

In summary, it is concluded that dust on Mars is likely to be a multicomponent mixture of weathered and non weathered minerals. Smectite clays are suggested as major components among the weathered minerals, assumed to be adsorbed and coated with amorphous iron oxyhydroxides and mixed with small amounts of better crystallized iron oxides (ferrihydrite, goethite and hematite) as separate phases, but having extremely small crystal sizes. As accessory minerals it is likely that the dust contains various sulfate minerals (Kieserite ( $\text{MgSO}_4 \cdot \text{H}_2\text{O}$ ) and/or anhydrite ( $\text{CaSO}_4$ )). If present, carbonates are likely to be at very low concentrations, although siderite ( $\text{FeCO}_3$ ) may be present at somewhat higher concentrations. The chemical reactivity of this multicomponent system is complex to predict. It may be dominated by the ability of the smectite clays to adsorb volatiles due to their extensive surface area (up to 800  $\text{m}^2/\text{g}$ ) and their catalytic reactivity in chemical and photochemical reactions. Furthermore, it is likely that the presence of the nanocrystalline iron oxy-hydroxy particles, with their large surface area, will increase the adsorption capacity of the system and enhance its reactivity.

REFERENCES: 1) Hunt, G.R. et al.(1973) Icarus 18,459-469. 2) Toon, O.B. et al. (1977) Icarus 30, 663-696. 3) Clark, B.C. et al. (1977) JGR 82, 4577-4594. 4) Toulmin, P. III et al. (1977) JGR 82, 4625-4634. 5) Banin, A. and Rishpon, J. (1978) Life Sci. Space Res. 17, 59-64. 6) Banin, A. and Rishpon J. (1979) J. Mol. Evol. 14, 133-152. 7) Banin, A. et al. (1985) JGR 90, C771-C774. 8) Banin, A. (1986) "Clays on Mars" in Clays and the Origin of Life (H. Hartman and A.G. Cairns-Smith, eds.) pp 106-115, Cambridge Univ. Press. 9) Zolotov, M. et al. (1983) LPSC 14, 883-884. 10) Zolensky, M.E. et al. (1987) Mars Sample Return Workshop (Abst.) LPI/NASA/JSC, 96-97. 11) Allen, C.C. et al. (1981) Icarus 45, 347-369. 12) Singer, R.B. (1982) JGR 87, 10,159-10,168. 13) Adams, J.B. et al. (1986) JGR 91, 8098-8112. 14) Banin, A. and Margulies, L. (1983) Nature 305, 523-526. 15) Banin, A. et al. (1988) LPSC 19, 27-28. 16) Singer, R.B. et al. (1979) JGR 84, 8415-8426. 17) McCord, T.B. et al. (1982) JGR 87, 3021-3032. 18) Evans, D.L. and Adams, J.B. (1979) PLPSC 10, 1829-1834. 19) Evans, D.L. and Adams, J.B. (1980) PLPSC 11, 757-763.

Banin, A.

20) Morris, R.V. et al. (1983) LPSC 14, 526-527. 21) Burns R.G. (1986) Nature 320, 55-56. 22) Morris, R.V. (1987) In, Mars Sample Return Workshop LPI/NASA/JSC Workshop Abstracts 96-97. 23) Gerstl, Z. and Banin, A. (1980) Clays Clay Min. 28, 335-345. 24) Ben Shlomo, T. and A. Banin - unpublished data. 25) Schwertmann, U. (1988) in Iron in Soils and Clay Minerals (J.W. Stucki, B.A. Goodman and U. Schwertmann, eds.) pp. 267-308, D. Reidel, Dordrecht. 26) Singer, R.B. (1985) Adv. Space Research 5(8) 59-68. 27) Kahn, R. (1985) Icarus 175-190. (This work was supported in part by the NASA Exobiology and Solar Systems Exploration Programs).

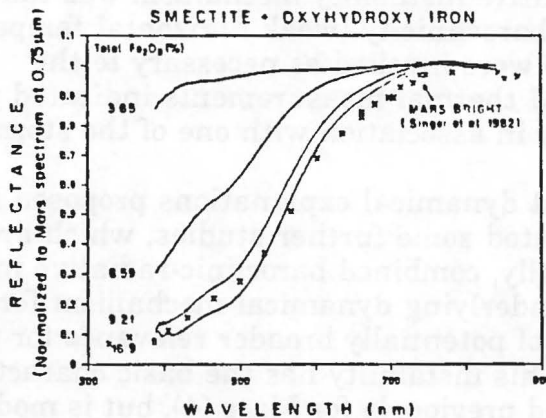


**Fig.1:** Reflectance spectra of Mars and of smectite (montmorillonite) clay loaded with various amounts of iron in an acidic environment. Spectroscopically these Mars soil analogs show reflectance similar to that of Mars soil at the wavelength range 0.4-0.85 $\mu$ m, due to oxyhydroxy-iron in poorly crystalline environments. Chemically, the highest level of iron-addition constitutes a full chemical analog of Mars soil with respect to iron content.

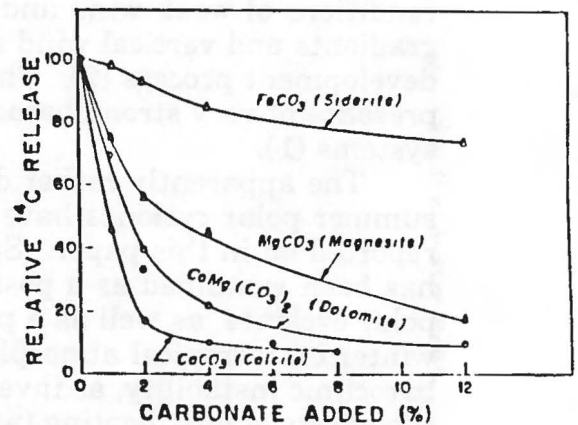


**Fig.2:** The effect of carbonate minerals on the reactivity of a Mars soil analog in the simulation of the Viking LR experiment on Mars. The analog, smectite-montmorillonite enriched to 100% ion exchange capacity, containing in total 6.5%  $Fe_2O_3$ , shows reactivity similar to the Mars Soil(6,8), and its decomposition capacity is taken as 100%. Additions of carbonate decrease the decomposition as measured by  $^{14}CO_2$  release. The effect of calcite is very significant even at low levels of additions, whereas siderite can be present at much higher concentrations without interfering with the reaction.

BAROCLINIC-RADIATIVE INSTABILITY AND MARTIAN SUMMER  
POLAR CYCLONES; J.R. Barnes, Department of Atmospheric Sciences,  
Oregon State University, Corvallis, OR 97331

Some of the more interesting atmospheric phenomena observed by Viking were the polar cyclones (or so-called "spiral clouds"), seen at high latitudes in the summer northern hemisphere in several orbiter images (1,2). Based on the similarity in appearance to terrestrial extratropical cyclones, as well as the observation of sharp nearby temperature gradients by the Viking IRTM, these were identified as being manifestations of baroclinic instability in the summer polar atmosphere (1). The relatively small horizontal scales of the polar cyclones (~ 100-300 km) were noted as constituting a difference from terrestrial analogs. In contrast with the interpretation of baroclinic instability, the polar cyclones were alternatively proposed as being a result of radiative instability (2). This instability, as fundamentally investigated earlier (3), would be driven by atmospheric heating due to the presence of dust. Both the images and IRTM data indicated that a dust haze was present in the region of the polar cyclones (1,2). A key difficulty with the radiative instability mechanism was that conditions of weak wind and weak baroclinicity (weak horizontal temperature gradients and vertical wind shears) were invoked as necessary to the development process (2). The IRTM thermal measurements indicated the presence of very strong baroclinicity in association with one of the storm systems (1).

The apparently rather different dynamical explanations proposed for the summer polar cyclones have motivated some further studies, which are reported on in this paper. Specifically, combined baroclinic-radiative instability has been examined as a possible underlying dynamical mechanism for the polar cyclones, as well as a process of potentially broader relevance for the winter extratropical atmosphere. This instability has the basic character of baroclinic instability, as investigated previously for Mars (4), but is modified by the effects of dust heating (which by themselves lead to a pure radiative instability).

A  $\beta$ -plane dynamical model like that used in linear baroclinic instability studies of the Martian atmosphere (4) has been employed for calculations of baroclinic-radiative instability. The effects of dust heating are simply parameterized in terms of the dust mixing ratio, which is determined according to a dust transport equation coupled to the dynamical model. The transport equation is the same (governing just the perturbation part of the dust field) as in earlier simulations of dust transport during a polar warming event (5). The coupled dynamical-dust transport model enables calculations of linear baroclinic-radiative instability to be made for relatively realistic basic states (zonal flows and dust distributions), with dissipation (radiative damping and surface friction). Without dust heating, the model yields unmodified baroclinic instability as examined previously (4). With dust heating, but without baroclinicity (that is, without vertical shear of the basic zonal flow), the model yields pure radiative instability fundamentally like that investigated earlier (2,3). In the presence of both dust heating and baroclinicity, combined

baroclinic-radiative instability can occur. It can be anticipated, on the basis of the relatively low growth rates for pure radiative instability (2), that the basic character of the combined instability will be that of baroclinic instability (for reasonably large baroclinicity and dust heating that is not overly strong). It will be modified, though, by the effects of the dust heating. The modification should be greatest at shorter horizontal scales. This aspect may be especially important for the relatively short scales of the summer polar cyclones.

Preliminary calculations with the model have been made, and some of the results will be reported on and discussed. Implications for the dynamics of the summer polar cyclones, as well as winter midlatitude disturbances, will be addressed.

### References

- (1) Hunt, G.E., and P.B. James (1979) Martian extratropical cyclones. *Nature*, **278**, 531-532.
- (2) Gierasch, P.J., P. Thomas, R. French, and J. Veverka (1979) Spiral clouds on Mars: A new atmospheric phenomenon. *Geophys. Res. Lett.*, **6**, No. 5, 405-408.
- (3) Gierasch, P.J., A.P. Ingersoll, and R.T. Williams (1973) Radiative instability of a cloudy planetary atmosphere. *Icarus*, **19**, 473-481.
- (4) Barnes, J.R. (1984) Linear baroclinic instability in the Martian atmosphere. *J. Atmos. Sci.*, **41**, 1536-1550.
- (5) Barnes, J.R. (1988) Transport of dust to high northern latitudes in a Martian polar warming. Submitted to *J. Geophys. Res.*

MARS OBSERVER VIMS AND PHOBOS KRFM-ISM OBSERVATIONS OF MARS DUST;  
L.W. Esposito, LASP/Univ. of Colorado

The visible and near-IR is a fruitful region to observe dust because of its substantial opacity at these wavelengths, compositional implications from near-IR bands, and the possibilities of volatiles coating the dust particles. Because of the varying strengths of CO<sub>2</sub> bands in this region, the total abundance of dust and its vertical distribution can be inferred from comparing the band strengths and shapes. This method is useful even at nadir viewing and thus it can measure larger columns of dust (such as during dust storms) that cannot be probed by limb viewing. The Mars Observer orbit and mission length allow global and seasonal variation in dust to be determined. The high spatial resolution of VIMS can identify heterogeneity and allow small storms to be studied. The KRFM-ISM experiment on PHOBOS has lower spatial and spectral resolution, but has the advantage of observing at a range of viewing and sun angles (further, it is now en route to Mars). KRFM bands up to 70 $\mu$  will further constrain dust size and distribution. If VIMS or a scaled-down spectrometer is a part of the Mars Observer science payload, valuable intercomparisons are expected.

**AN ASSESSMENT OF THE METEORIC AND METEORITIC CONTRIBUTIONS TO DUST ON MARS; G.J. Flynn<sup>1</sup>, and D.S. McKay<sup>2</sup>, (1) Dept. of Physics, SUNY-Plattsburgh, Plattsburgh, NY 12901, (2) SN14, NASA Johnson Space Center, Houston, TX 77058**

Four types of meteoric and/or meteoritic material should be found on Mars: 1) micrometeorites, many of which will survive atmospheric deceleration unmelted, which should fall relatively uniformly over the planet's surface, 2) ablation products from larger meteors and meteorites which ablate, break up and/or burn up in the Mars atmosphere, 3) debris from large, crater forming objects, which, by analogy to terrestrial and lunar impact events, will be concentrated in the crater ejecta blankets (except for rare, large events, such as the proposed C-T event on earth, which can distribute debris on a planetary scale), and 4) debris from the early, intense bombardment, which, in many areas of the planet, may now be incorporated into rocks by geologic processes subsequent to the intense bombardment era.

To estimate the extent of meteoritic addition to indigenous Martian material, the meteoritic flux on Mars must be known. Hartmann et al. (1981) estimate that the overall flux of large, crater producing objects at Mars is twice that for the Moon and 1.33 that for Earth. For small particles (< 100 micrometers in diameter), whose orbital evolution is dominated by Poynting-Robertson (PR) drag (Dohnanyi, 1978), we estimate the flux at Mars from the measured flux at Earth. The smaller Martian gravitational enhancement as well as the decrease in the spatial density of interplanetary dust with increasing heliocentric distance (inferred from the fall off of zodiacal light intensity) should reduce the flux of small particles at Mars to about 0.33 times the flux at Earth. Because of the smaller planetary cross-section the total infalling mass at Mars is then estimated to be 0.09 times the infalling mass in the micrometeorite size range at Earth.

**INFALL ASSESSMENT:** At Earth the current annual infall of meteoric and meteoritic material hitting the top of the atmosphere is estimated, from satellite, radio and photographic meteor measurements, at 16,000 tons, with 12,400 tons of that concentrated in the particles in the  $10^{-6}$  to  $10^{-2}$  gram mass range (Hughes, 1978). Its accumulation rates in sea sediments suggest a relatively constant meteoritic and meteoric infall on earth over the past 67 million years (Kyte, 1986), though Kyte infers a long-term infall rate of  $77,000 \pm 25,000$  tons per year, about five times the current infall estimated by Hughes (1978). The  $10^{-6}$  to  $10^{-2}$  gram particles (from 100 to 3000 micrometers in diameter for density  $1 \text{ gm/cm}^3$ ), which contribute 75% of the extraterrestrial material, are somewhat larger than the size whose orbital evolution is dominated by PR drag. The Mars flux of these particles is thus likely to be between that which we calculate for PR drag dominated particles and that suggested by Hartmann et al. (1981) for the larger objects. Taking the 0.09 reduction factor we calculate for the smaller particles as a lower limit for the Mars/Earth infall ratio for  $10^{-6}$  to  $10^{-2}$  gram particles, and using the lower value of the Earth infall rate from Hughes (1978), a minimum of approximately 1100 tons of meteoritic material in the  $10^{-6}$  to  $10^{-2}$  gram mass range would be deposited on the top of the Martian atmosphere annually. If this mass reached the surface as solid material, it would be sufficient to cover the planet with a 3 to 4 cm thick layer over the age of the solar system. This micrometeoritic infall amounts to about  $0.7 \text{ cm}/10^9$  years. Substantially larger values are possible if either the Hartmann et al. Mars/Earth flux ratio or the higher Kyte earth flux is adopted, with an accumulation of about  $14 \text{ cm}/10^9$  years resulting if both values are used.

**DIRECT COLLECTION:** On earth, particles in the  $10^{-6}$  to  $10^{-2}$  gram mass range are normally melted or volatilized on atmospheric entry, with only particles  $\leq 100$  micrometers in diameter surviving entry relatively unaltered (Brownlee, 1985). *However Mars, because of its low gravitational acceleration combined with sufficient atmospheric density to provide deceleration, is probably the most favorable site in the solar system for unaltered survival (and thus collection) of micrometeorites.* We have made new calculations of the interactions of these micrometeorites with the Martian atmosphere using the micrometeorite deceleration model first used by Whipple (1950) and the upper atmospheric density profile for Mars derived from Viking entry measurements (Seiff and Kirk, 1976). Particles of the same density, shape, and thermal characteristics entering at velocities near the Martian escape velocity are heated to a peak temperature only half that experienced on Earth entry at earth escape velocity. Although most particles larger than 75 to 100 micrometers in diameter are melted on Earth atmosphere entry, the cutoff size for melting on Mars entry would be about 13 times larger, or 1000-1300 micrometers in diameter.

The concentration of micrometeorites in Martian soils depends on the fraction of them which survive atmospheric entry as solid material (either unmelted, as are the micrometeorites collected from the Earth's stratosphere, or melted, as are the chondritic spheres collected from the sea sediments - see

review by Brownlee (1985)), as well as the Martian regolith depth, and the total accumulation time. For illustrative purposes, we assume that all of the micrometeorites smaller than 3000 micrometers survive atmospheric entry in some form as solid material, the Martian regolith has an average depth of 10 m (consistent with Arvidson's (1986) estimate of a planetary erosion rate of meters/ $10^9$  years, based on crater preservation), and that micrometeorites have been accumulating at the present estimated rate for the past  $4 \times 10^9$  years. For these conditions, a 10 gram average soil sample would have been mixed with about 5000 micrometeorites greater than 100 micrometers in diameter and 10 micrometeorites greater than 800 micrometers in diameter. Micrometeorites in this size range which have survived atmospheric entry are normally not collected at earth. Since these larger particles from Mars orbital distance are likely to sample different sources than the smaller micrometeorites collected at 1 a.u. in the cosmic dust sampling program on earth (Flynn, 1988; Zook and McKay 1986), returned Mars soils may provide a unique resource for micrometeorite analysis.

**MICROMETEORITES AS A TOOL:** The degree to which Martian weathering will break down micrometeorites is unknown. However, since unmelted 1000 micrometer fragments of meteoritic material have been identified in the 2.3 million year old Pliocene layer on Earth (Brownlee et al., 1982), micrometeorites added to Martian regolith after atmospheric deceleration below hypervelocities may still be identifiable by petrographic or chemical means. *Assuming that micrometeorites could somehow be identified in returned soil samples, this addition of micrometeorite material to the uppermost Martian regolith at a constant rate could conceivably provide a powerful tool for tracking rates of erosion, deposition, and weathering.* On Mars sample return missions, an attempt should be made to collect soils from different geologic sites (catch basins, lag surfaces, flat high plains, valley bottoms, etc.) so as to provide a variety of soils of different sedimentary environments. One of the important differences among these environments might be the proportion of petrographically or chemically identifiable micrometeorites mixed into the soil.

**COLLECTING SITES FOR MICROMETEORITES:** Martian surface processes (weathering and wind erosion, transport, and deposition) may fractionate the dust by size, density or composition providing regions of increased local concentration, suggesting even more suitable sites for micrometeorite sampling than the average soil. *These sites may include placer catch basins or lag surfaces which may accumulate high density micrometeorites or their derived and altered minerals. Conversely, low density micrometeorites may be wind segregated along with finer Martian dust and may constitute a relatively coarse-grained component of that dust at its deposition sites.* By analogy with Antarctica, meteorites of all size ranges may be relatively concentrated in Martian polar regions, although the concentration mechanisms may be different.

**CHEMICAL SIGNATURES:** The possibility that detectable micrometeorites and their remains can be found in the Martian soils depends on the relative rates of infall, weathering and alteration, transportation, and mixing. These rates are not yet known reliably enough to allow us to predict with certainty whether identifiable micrometeorites will be found. While they may be relatively quickly destroyed by Martian weathering, the chemical signature, particularly siderophiles and volatiles, may persist in the soils, as they have in the lunar regolith (Anders, et al., 1973). If the regolith production rate on Mars is of order 1 meter/ $10^9$  years, our calculated infall rate would give rise to a mean concentration of about 1% micrometeoritic material in the regolith.

In the lunar case the composition of the non-indigenous material was taken as the residual after subtracting rock composition from soil composition. Two meteoritic components were detected. In mature soils the residual has a trace element composition consistent with the addition of 1.5% CI meteoritic material, attributed to the long term micrometeorite infall (Anders et al., 1973). Less mature highland soils also show a second component, characterized by fractionated siderophile content and low volatiles, attributed to ancient bombardment (Anders et al., 1973).

Boslough (1988) and Clark and Baird (1979), applying the subtraction method to the Viking chemical data, suggest the Mars regolith can be fit by a mixture of 40% CI meteorite and 60% planetary rock fragments. Boslough (1988) suggests the meteoritic component is ancient. But it could equally well be the micrometeorite component, which dominates the ancient component in lunar soils. If either the planetary regolith production rate is significantly lower than the 1 meter/ $10^9$  year value we have used for illustrative purposes or if the micrometeorite infall is higher than we calculate using conservative values for the earth flux and the infall ratio, the fraction of meteoritic material would increase from the 1% we calculated. Increasing the earth infall rate to the value reported by Kyte (1986) and the Mars/Earth infall

ratio to the Hartmann et al. (1981) value, and reducing the Mars erosion rate to one-third of the 1 meter/10<sup>9</sup> years would produce a micrometeorite concentration in the Martian regolith of about 40%. Thus a Martian regolith containing a substantial fraction of meteoritic material cannot be ruled out. On earth the Ni/Fe ratio and the Ir abundance have proven to be diagnostic indicators of meteoritic material, since Ir and Ni are enriched in CI meteorites but depleted in crustal materials. Direct measurement of the Ni and/or Ir abundances in the Mars regolith should help determine the meteoritic content of the regolith.

The micrometeorites collected at Earth, because of their small size, contain large concentrations of solar wind implanted ions, particularly the noble gases (Hudson et al., 1981; Rajan et al., 1977) and likely hydrogen. These solar wind species, carried into the Martian regolith by the micrometeorites, may also perturb the bulk chemical abundances.

**MARTIAN AGGLUTINATES:** If, as we calculate, micrometeorites are all slowed down by the Martian atmosphere, and assuming that most lunar agglutinates are made by micrometeorite impacts, no analogous Martian agglutinates would be expected (unless there were an era in which the atmosphere was considerably less dense than at present). However, many types of impact glasses would be expected from larger impacts, and some of these glasses may resemble lunar agglutinates in some respects.

**MARTIAN SOIL MATURITY:** Gault and Baldwin (1970) have estimated a minimum impact crater size of 50 meters, taking into account fragmentation and ablation of the incoming projectiles as well as atmospheric deceleration. The smallest craters noted in Viking orbiter images are about 100 meters in diameter (Blasius, 1976), but smaller craters beyond the resolution limit of the photographs may still be present. Dycus (1969) predicts that projectiles as small as 10 gm would still form craters. However, craters too small to be seen from the orbiter are not apparent in Viking lander images. Impact gardening associated with the 50 meter and larger craters predicted by Gault and Baldwin (1970) would determine regolith turnover rates and cause comminution of rocks into soils. The addition of micrometeorites would affect the petrology and chemistry of Martian soil. Weathering and sedimentary processes on Mars would also process the regolith components. The overall effect would be to make an exceedingly complex regolith. *A new maturation scale will be necessary for Martian regolith. This scale will have to include terms which reflect (1) impact reworking, (2) addition of micrometeorites, and (3) Martian surface weathering and alteration.* For example, if concentration mechanisms can be factored out, the abundance of micrometeorites (identified petrographically or chemically) in a soil layer might be directly related to its near-surface exposure time in a manner analogous to the abundance of agglutinates in lunar soils. In addition to soil evolution through maturation, physical mixing of soils of differing maturities should be common.

**CONCLUSIONS:** *The addition of meteoritic material to the Martian regolith could significantly perturb the chemical abundances in the soils, particularly the abundances of volatile and siderophile elements which are abundant in CI meteorites but depleted in crustal materials, and of noble gases (and possibly hydrogen) which are implanted in the micrometeorites during space exposure and carried into the soils with the particles. The first returned soil samples from Mars should provide the opportunity for recovery and analysis of unaltered micrometeorites larger than any sampled on earth, assessment of the magnitude of the meteoritic component, and possibly an estimate of the rate of erosion and regolith production on the planet.* This micrometeorite population may be quite different from the population sampled at 1 a.u. The extent of regolith gardening, small crater production and agglutinate production, if any, will also provide clues to the evolution of the Martian atmospheric density over time.

**REFERENCES:** Anders, E. et al. (1973) Moon, 8, 3-24.; Arvidson, R.E. (1986) in Dust on Mars II, LPI Tech. Report 86-09, 9.; Blasius, K.R. (1976) Icarus, 29, 343-361.; Boslough, M.B. (1988) LPSC XIX, 120-121.; Brownlee, D.E. (1985) Ann. Rev. Earth Planet. Sci. 1985, 295-335.; Brownlee, D.E., et al. (1982) LPSC XIII, 69-70.; Clark, B.C. and Baird, A.K. (1979) JGR, 84, No. B14, 8395-8403.; Dohnanyi, J.S. (1978) in Cosmic Dust (ed. J.A.M. McDonnell) Wiley, New York, 527-605.; Dycus, R. F. (1969) Publications of the Astronomical Soc. of the Pacific, 81, 399-414.; Flynn, G.J. (1988) Atmospheric Entry Heating: A Criterion to Distinguish Between Asteroidal and Cometary Sources of Interplanetary Dust, Icarus, in press.; Gault, D.E., and Baldwin (1970) EOS Trans. AGU, 51, 343.; Hartmann, et al. (1981) in Basaltic Volcanism on the Terrestrial Planets, LPI, p 1049-1127.; Hudson, B. et al. (1981) Science, 211, 383-386.; Hughes, D.W. (1978) in Cosmic Dust (ed. J.A.M. McDonnell) Wiley, New York, 123-185.; Kyte, F.T. (1986) LPSC XVII, 452-453.; Rajan, et al. (1977) Nature, 267, 133-134.; Seiff, A. and Kirk, D. B (1976) Science, 194, p.1300-1302.; Whipple, F. L. (1950) Proc. Nat. Acad. Sci., 36, p.687-695.; Zook, H.A. and McKay, D.S. (1986) LPSC XVII, 977-978.

**ACKNOWLEDGEMENTS:** This work was supported in part by NASA Grant NAG 9-257 and a NASA/ASEE Summer Faculty Fellowship to GJF.

**POSSIBLE INTENSE VORTICES AND THE POTENTIAL FOR DUST AND SAND TRANSPORT ON MARS; J.A. Grant and P.H. Schultz, Geological Sciences, Brown University, Providence, RI 02912**

**INTRODUCTION:** Characteristics of distinct, dark, ephemeral filamentary lineations in certain locations on Mars and their occurrence only during specific seasonal atmospheric conditions indicate they result from intense atmospheric vortices (1). Similar markings have been interpreted as linear seif dunes (2) or joint patterns (3), but these explanations are inconsistent with all observations. If atmospheric vortices of up to tornadic intensity do exist on Mars they should be capable of lofting and transporting significant amounts of dust and sand-sized material (4).

**DESCRIPTION:** Individual lineations have total lengths ranging from 2 km to over 75 km and widths up to a few hundreds of meters (Fig. 1). They have well defined, straight to curvilinear plans that commonly cross each other and traverse considerable relief. At the highest resolution available (~75 m/pixel) no relief on the lineations has been identified. While the majority are found within several midlatitude areas in the southern hemisphere, their occurrence is quite widespread (but rare near the equator). The lineations develop with a predominantly E-W or NE-SW orientation on stripped intercrater plains and the floors of some large craters during the late summer: they then are rapidly modified and become undetectable by midfall (1). Lineations appear to redevelop in the same broad areas from year to year, but the location of individual lineations within these areas changes.

**DISCUSSION:** As summarized in (1), the lineations are not thought to be the expressions of joints or dunes (2,3) because the markings: (A) are highly variable in occurrence over short time scales; (B) traverse landforms, each other, and local structural trends, without deflection or interruption (Fig. 1); (C) change position from year to year; (D) are insensitive to broad scale structural trends; (E) are orders of magnitude larger than most terrestrial joints; (F) have grossly similar orientations over broad areas; and (G) cross materials whose competence should be too low for joint expression (i.e. ejecta facies). The occurrence and characteristics of all of the lineations indicate that they result from surface scour and re-deposition of material during the passage of intense atmospheric vortices (1). Considerable fine-grained material would be lofted and carried along by these vortices thereby leaving a stripped, coarser grained surface lag. Coarser sand-sized material also should be lifted (4), but would experience more limited transport. The resultant bands of relatively coarse-grained material remaining behind the intense vortices would be dark compared to the surrounding, unaffected areas (5).

Although the occurrence of dust devils on Mars has been confirmed (6) it is unlikely that they are responsible for the formation of the lineations. First, the size (length and width) and some of the characteristics of the martian lineations are inconsistent with those of martian and terrestrial dust devils (1,6,7). Second, the observed martian dust devils did not produce surface lineations. And third, atmospheric conditions present during formation of the lineations are not optimal for dust devil formation.

Martian lineations begin to form in late summer following dust storm activity (1) when the clearing atmosphere allows development of a deep convective layer (8). The occurrence of this deep convective layer in combination with unstable atmospheric conditions (1) and the onset of seasonal baroclinic wave passage (9-11) establish conditions similar to those on the Earth favoring tornadogenesis (12). Consequently, strong atmospheric vortices of possible tornadic-intensity might also form on Mars (1). While terrestrial tornadoes are driven by latent heat released by water condensation, martian

vortices would be driven primarily by extended dry convective uplift of unstable surface air in the deep convective layer. Only a minor contribution at most would be made by latent heat release due to the paucity of water in the martian atmosphere (13,14). Because these intense vortices are controlled by midlevel rather than near-surface atmospheric processes (12), they would be less sensitive to topography than dust devils and therefore more likely to produce groundtracks which traverse landforms and have gaps unrelated to topography. Finally, terrestrial tornadic vortices generate surface markings that resemble the martian lineations (12).

The apparent absence of lineations on Mars during the spring when similar atmospheric conditions exist may be related to the scarcity of images in those locations where they are expected to form (1). Complete destruction of the lineations by midfall is likely the result of burial by dust from atmospheric fallout including processes associated with the expanding seasonal polar cap (1).

**IMPLICATIONS:** From the distribution of lineations we estimate that they form seasonally in areas covering roughly  $1.7 \times 10^6 \text{ km}^2$ , or about 1.2% of the surface of Mars with the largest fraction (>82%) occurring between 30°S and 65°S. The average lineation density (55 to 60 per thousand square kilometers) in the latter areas combined with their average width (-200 m) and length (-10 km) represents about  $2 \times 10^5 \text{ km}^2$  total area and permits an estimate of the seasonal eolian transport by this processes. A value for the average erosion resulting from the passage of a martian intense vortex of 1 mm was utilized in these calculations since measurements of the load carried by intense vortices on the Earth are not readily available. The area of each track multiplied by the amount of erosion gives a total average dust and sediment load of  $2 \times 10^3 \text{ m}^3$  entrained by each vortex over a distance of 10 km with the maximum mass lofted about  $4.0 \times 10^3 \text{ kg/vortex}$  (for material density of  $-2.2 \text{ g/cm}^3$ ). For comparison, the load carried by martian dust devils has been estimated to be  $3 \times 10^3 \text{ kg}$  each based on their optical depth (6). The value given for the load carried by each martian intense vortex is the sum for the entire path-length travelled. The load carried by a single intense vortex at any moment should be less than the maximum mass predicted because much of the entrained fine grained material (<5-10 microns) will be lost through the top of the vortex while some of the coarser material will simply be redeposited along the track. For the total area seasonally covered by lineations as much as  $0.18 \text{ km}^3$  of dust and sediment could be lofted over a short period during late summer.

The fine grained fraction lofted by these vortices may serve to prolong the decay of large martian dust storms or possibly contribute to their redevelopment. If intense vortices also develop during the southern hemisphere spring as analogues to seasonal tornadogenesis on the Earth, then they could play an important role in the initial development of certain large dust storms. Dust lofted in the Hellespontus region could contribute directly to dust storm development while dust raised in midlatitudes further to the west may have to drift north towards Solis planum before contributing to development. Lofted materials of all sizes would be transported away from source areas where the intense vortices develop. While fine grained material could contribute directly to the formation of polar layered terrains, coarser material could accumulate on crater floors and in the circumpolar dune fields, subsequently reworked by other winds to form dunes.

Although the seasonal erosion due to intense vortices on Mars will be small, the cumulative yearly erosion could be significant. Such vortices may be responsible for much of the stripped appearance of the northern martian plains, but the lower albedo produced by removal of the finer material may preclude detection of the lineations there.

REFERENCES: (1) J.A. Grant and P.H. Schultz, *Science*, 237, 883 (1987). (2) J.A. Cutts and R.S.U. Smith, *J. Geophys. Res.*, 78, 4139 (1973). (3) J. Veveraka, *Icarus*, 27, 495 (1976). (4) R. Greeley, B.R. White, J.B. Pollack, J.D. Iverson and R.N. Leach, *Geol. Soc. Am. Spec. Pap.*, 186, 101 (1981). (5) P.R. Christensen and H.H. Kieffer, *J. Geophys. Res.*, 84, 8233 (1979). (6) P. Thomas and P.J. Gierasch, *Science*, 230, 175 (1985). (7) L. Ives, *Bull. Am. Met. Soc.*, 28, 168 (1947). (8) C.B. Leovy, *Sci. Am.*, 237, 34 (1977). (9) M.H. Carr, *The Surface of Mars* (Yale Univ. Press, New Haven, CT, 1981). (10) R.M. Haberle, *Sci. Am.*, 254, 54 (1986). (11) J.A. Ryan et al., *Geophys. Res. Letts.*, 5, 715 (1978). (12) R.P. Davies-Jones, *In Thunderstorms: A Social, Scientific, and Technological Documentary*, Vol. 2, 2 ed. (E. Kessler, Ed) 197-236 (Univ. of Oklahoma Press, Norman, OK, 1985). (13) D.W. Davies and L.A. Wainio, *Icarus*, 45, 216 (1981). (14) C.B. Farmer and P.E. Doms, *J. Geophys. Res.*, 84, 2881 (1979).

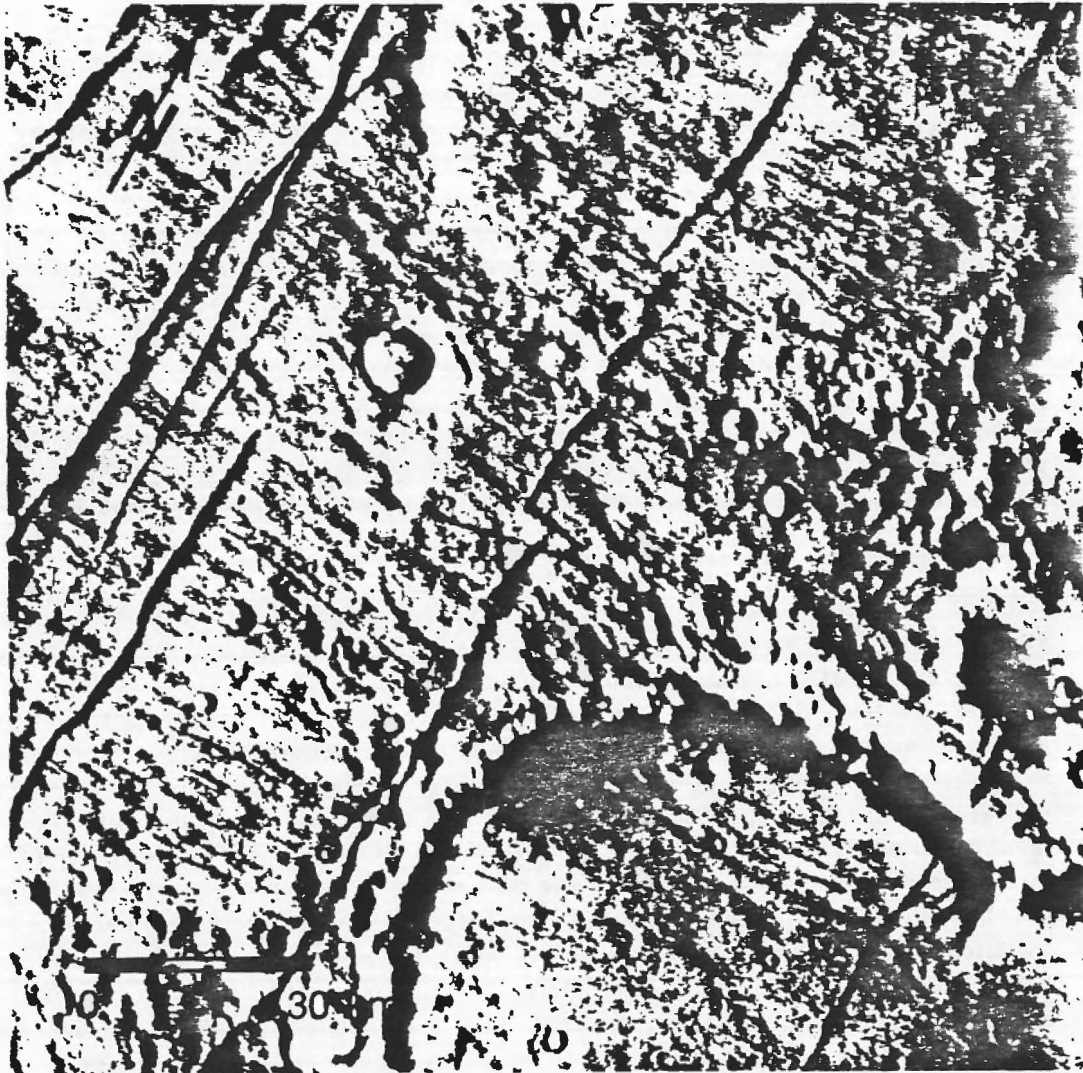


Fig. 1. Filamentary lineations located at 91°W, 48.5°S just over 1000 km west of Argyre basin. Lineations trend E-W across the image and cross both crater walls and large N-S oriented fractures. Viking image 523A34.

**COMPARISON OF MARTIAN AEOLIAN FEATURES AND RESULTS FROM THE GLOBAL CIRCULATION MODEL; R. Greeley, A. Skyeck, Dept. of Geology, Arizona State University, Tempe, AZ 85287-1404, and J.B. Pollack, NASA-Ames Research Center, Moffett Field, CA 94035.**

aeolian (wind) processes link the atmosphere of a planet with its surface. Wind is apparently the dominant agent of surface modification on Mars today, as evidenced by frequent dust storms. Features attributed to aeolian processes include dunes, yardangs, grooves, deflation pits, and albedo patterns that are time-variable. In addition, vast regions appear to be mantled with sediments presumably deposited from the atmosphere. Because of the common occurrence of aeolian features on Mars and the frequent occurrence of dust storms, understanding the nature of the features and of the interaction between the atmosphere and lithosphere are critical for several aspects of martian science: (1) the presence or absence of active and inactive dust mantles may affect the interpretation of some remote sensing data for Mars, (2) the location and occurrence of aeolian deposits will strongly influence the selection of potential landing and sample return sites, and (3) interpretation of martian surface evolution must include the identification and separation of material units formed by a wide variety of processes (fluvial, periglacial, volcanic, etc.).

Some surface features can be used to infer wind directions and strengths. For example, Ward et al. (1985) described yardangs oriented with the prevailing winds at the time of formation. However, they noted several "sets" of yardang orientations and suggested that there had been shifts in wind patterns with time. Wind streaks probably constitute the best "wind vanes". As described by Thomas (1982) and others, many wind streaks change with time and may reflect seasonal shifts in wind patterns. Wind streaks and the interpretation of wind patterns have been relatively well documented by Sagan et al. (1973), Thomas et al. (1981), Veverka et al. (1977), Greeley et al. (1977), and others. Incorporation of Viking IRTM data have enabled assessment of sediment sources, transport paths, and deposition sites of windblown sediments (Christensen, 1986; Lee, 1986). Dunes occur in high to mid latitudes (Breed et al., 1979; Thomas, 1982) and in small fields in equatorial regions. Although most are crescentic and barchan types (Breed et al., 1979; Tsoar et al., 1979) indicating a unidirectional wind regime, reversing winds were also suggested by Tsoar et al. (1979). Cutts and Smith (1973) and Lancaster and Greeley (1987) identified reversing and star-like dunes in some areas, suggesting seasonal changes in wind direction. However, the relationship between dune patterns and formative winds remains uncertain and there is poor agreement between the alignment patterns of the dunes and some models of wind patterns (Ward and Doyle, 1983). This may suggest that the dunes formed when martian wind regimes were different. Breed et al. (1979) suggest that some North Polar dunes are eroding today, or being modified under long-term changes in wind regimes; Tsoar et al. (1979) and Ward and Doyle (1983) suggest that some dunes are currently active. Thomas (1981) suggests southern hemisphere dunefields are aligned with current winds.

Important questions remain about the nature of dunes and other aeolian features on Mars and their relationship to past and present winds. The Global Circulation Model (GCM) developed by Pollack et al. is a complex simulation of the martian atmosphere based on Toon et al. (1980). Among the parameter predictions made by this simulation are predictions of wind surface shear stress. A program running on the Cray 2 computer allows predictions to be made for the wind surface shear stress as a function of atmospheric temperature and pressure, location on Mars, and other parameters such as topography, atmospheric dust-loading, and local surface roughness. Output from the program includes maps with wind vectors and strengths for stated conditions of martian season and climate. The magnitude, position, and azimuth of the GCM stress vectors are read from tape and are projected to a mercator base map. Wind streak and other aeolian data are digitized from published maps. The position and azimuth of these data are then calculated and projected to match the base map. Map symbols representative of aeolian features (bright streak, dark streak, yardang, etc.) are then drawn.

Figure 1 shows the GCM surface stress data and digitized bright streak data plotted on a mercator base map. The GCM data are arranged in  $7.2^\circ$  latitude by  $9.0^\circ$  longitude bins. The wind barbs indicate the direction and magnitude of the surface stress, and represent averages of discrete stress values produced for the simulated period:  $L_S = 281.02 - 286.73$ , sampled at 1.5 hour increments. The bright arrows indicate downwind direction as revealed by bright streak orientation. The aeolian data used for Figure 1 are bright streak azimuths digitized from a global compilation of aeolian features by Ward et al., 1985. The results from these comparisons will enable the following questions to be addressed: (1) Is there an alignment of aeolian features with predicted wind directions?, (2) Do erosional features occur in areas of predicted strong winds?, (3) Do aeolian depositional features occur in areas of low winds?, and (4) Do the GCM transport paths correspond to trends suggested by sediment transportation derived from IRTM studies such as Christensen (1983, 1986) and Lee (1986).

### References

- Breed, C.S., M.J. Grollier, and J.F. McCauley, 1979, Morphology and distribution of common "sand" dunes on Mars: Comparison with the Earth, *J. Geophys. Res.*, 84, 8183-8204.
- Christensen, P.R., 1986, Dust deposition and erosion on Mars: Cyclic development of regional deposits, *MECA Workshop on Dust on Mars II, LPI Tech. Rept. 86-09*, 14-16.
- Cutts, J.A. and R.S.U. Smith, 1973, Eolian deposits and dunes on Mars, *J. Geophys. Res.*, 78 (20), 4139-4154.
- Greeley, R., R. Papson, and J. Veverka, 1977, Crater streaks in Chryse Planitia region of Mars: Early Viking results, *Icarus*, 34, 556-567.
- Lancaster, N. and R. Greeley, 1987, Mars: Morphology of southern hemisphere intracrater dunefields, *Repts. Planetary Geology Geophysics Program - 1986, NASA TM-89810*, 264-265.
- Lee, S.W., 1986, Viking observations of regional sources and sinks of dust on Mars, *MECA Workshop on Dust on Mars II, LPI Tech. Rept. 86-09*, 44-45.
- Sagan, C. J. Veverka, P. Fox, R. Dubisch, R. French, P. Gierasch, L. Quam, J. Lederberg, E. Levinthal, R. Tucker, B. Eross, and J.B. Pollack, 1973, Variable features on Mars, 2, Mariner 9 global results, *J. Geophys. Res.*, 78, 4163-4196.
- Thomas, P., 1981, North-south asymmetry of eolian features in martian polar regions: Analysis based on crater-related wind markers, *Icarus*, 48, 76-90.
- Thomas, P., 1982, Present wind activity on Mars: Relation to large latitudinally zoned sediment deposits, *J. Geophys. Res.*, 87, 9999-10008.
- Toon, O.B., J.B. Pollack, W. Ward, J.A. Burns, and K. Bilski, 1980, The astronomical theory of climate change on Mars, *Icarus*, 44, 552-607.
- Tsoar, H., R. Greeley, and A.R. Peterfreund, 1979, Mars: The North Polar Sand Sea and related wind patterns, *J. Geophys. Res.*, 84, 8167-8180.
- Veverka, J., P. Thomas, and R. Greeley, 1977, A study of variable features on Mars during the Viking primary mission, *J. Geophys. Res.*, 82, 4167-4187.
- Ward, A.W. and K.B. Doyle, 1983, Speculation on martian north polar wind circulation and the resultant orientations of polar sand dunes, *Icarus*, 55, 420-431.
- Ward, A.W., K.B. Doyle, P.J. Helm, M.K. Weisman, and N.E. Witbeck, 1985, Global map of eolian features on Mars, *J. Geophys. Res.*, 90(B2), 2038-2056.

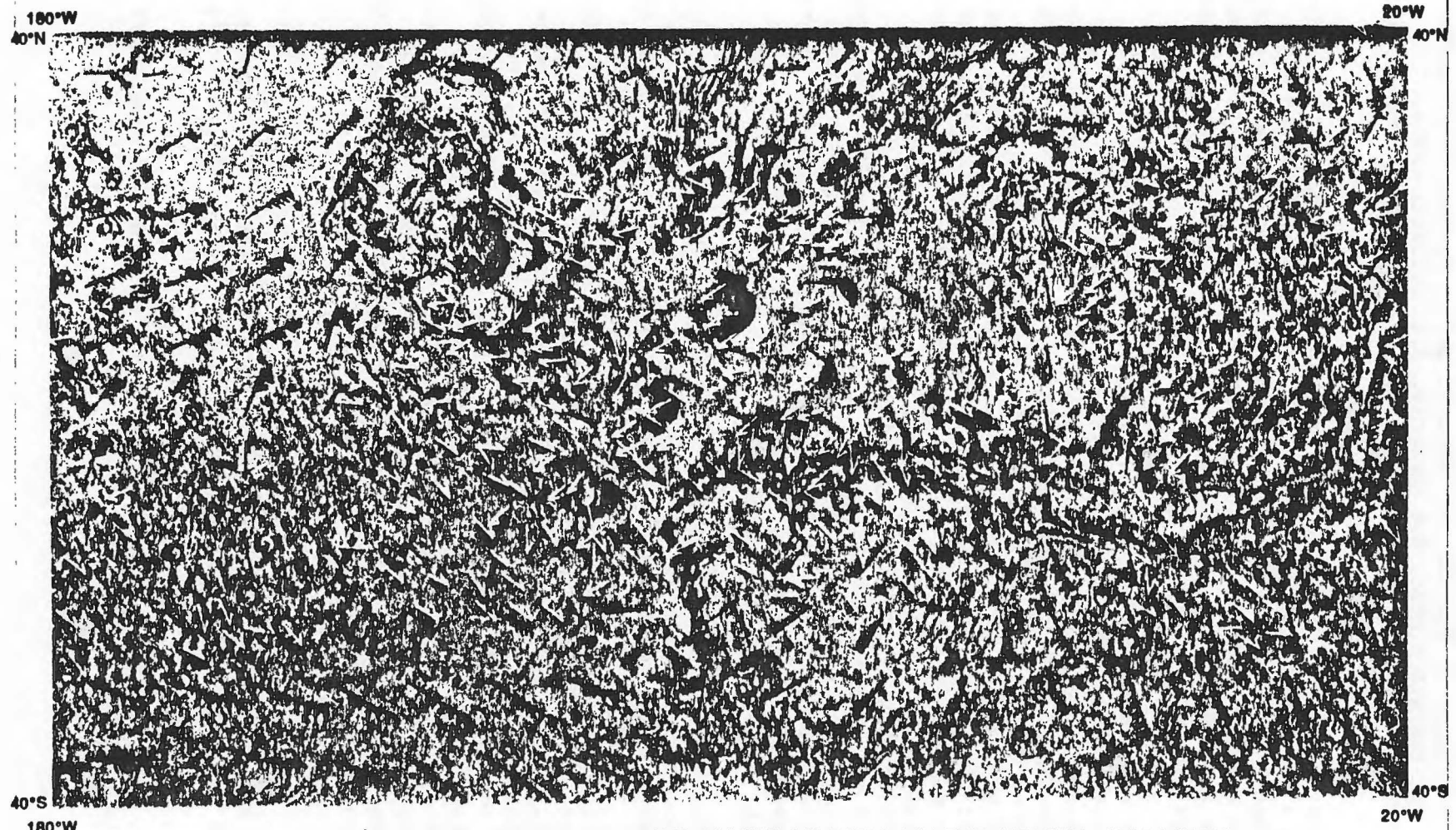


**Figure 1. GLOBAL CIRCULATION MODEL AND BRIGHT STREAK DATA FOR THE THARSIS REGION**

**GCM Parameters:**  
 Ls (deg) 281.02 - 286.73  
 Sampling increment - 1.5 hours  
 Stress averages for the simulation  
 are displayed.

**Wind barb explanation:**  

 stress units -  $N/m^2 \times 10^{-4}$   
 short dash - 5 units  
 long dash - 10 units  
 triangle - 50 units

Bright streak symbols indicate  
 inferred down-wind direction,  
 data from Ward et al., 1985.  
 (white) 

SIMULATIONS OF THE MARTIAN BOUNDARY LAYER: FACTORS CONTROLLING THE BEHAVIOR OF THE SURFACE STRESS; R.M. Haberle, J.B. Pollack, and J. Schaeffer, Space Science Division; NASA/Ames Research Center, Moffett Field, CA, 94035.

We have begun to explore the properties of the Martian atmospheric boundary layer using a one-dimensional (height) time-dependent second-order turbulence closure model that accounts for the radiative heating properties of suspended dust particles and CO<sub>2</sub> gas. Our goal in developing the model is to better understand the processes controlling the exchange of dust and water between the surface and atmosphere.

At last year's DPS meeting, we presented results which demonstrated the model's ability to reproduce the basic features of the diurnal variation of wind and temperature as measured at the Viking lander 1 site during summer (1). We also showed that this diurnal variation was sensitive to dust in the atmosphere. Of greatest interest in this regard was the diurnal variation of the surface stress (Figure 1). It was found that for a given wind speed at the top of the boundary layer, the amplitude of the diurnal variation in surface stress changed little for modest dust loadings (solar optical depths  $\leq 1$ ), but was substantially reduced as the opacity approached values typical of mature global dust storms (5 or so). This suggests that the change in static stability within the boundary layer due to dust heating provides a negative feedback to the dust raising process. This, of course, is not a new idea having been suggested earlier by others (2,3). However, as far as we know, our calculations represented to the first attempt, to quantify the effect.

A problem with these early calculations is that they were carried out only for the Viking 1 lander site during summer, for one assumed value of the wind speed at the top the boundary layer (15 m/sec), and for one set of soil properties. In addition, the surface heat flux calculation ignored the effect of molecular conduction near the surface, an effect that Sutton et al. (4) found to be potentially important for Mars. At the Dust III workshop, we plan to present results from a variety of simulations that examine more fully the behavior of the surface stress and other boundary layer parameters, and which include the effects of molecular conduction near the surface. The simulations will focus on southern subtropical latitudes during the dust storm season. Among the parameters to be varied are dust, free atmosphere wind speed, surface roughness, and soil thermal inertia. Insight gained from these simulations should be useful for interpreting the results of the Mars General Circulation Model.

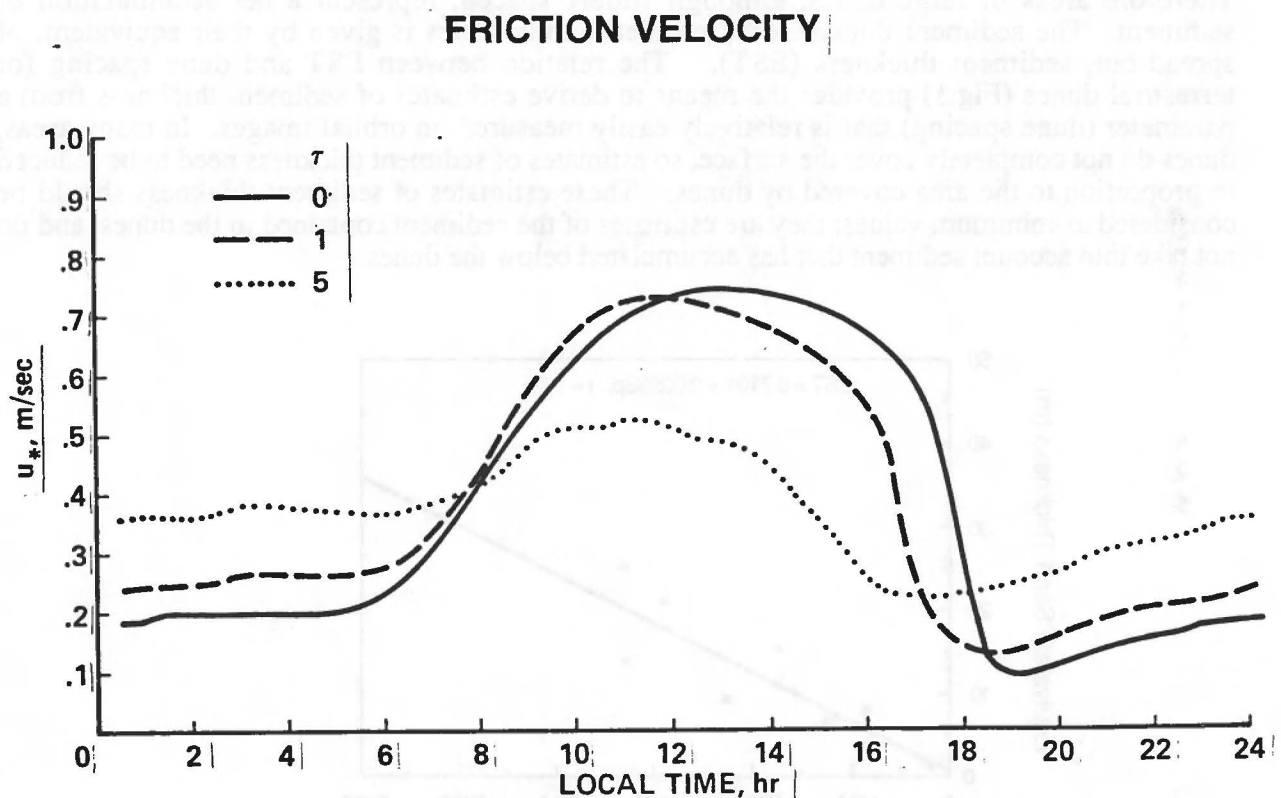
#### REFERENCES:

1. Haberle, R.M. and R. Hertenstein (1987). The Influence of Dust on the Structure of the Diurnally Varying Boundary Layer on Mars, BAAS, Vol. 19, 815.
2. Gierasch, P.J., and R.M. Goody (1973). A Model of a Martian Great Dust Storm. J. Atmos. Sci., 30, 169-179.

3. Leovy, C.B., Zurek, R.W., and J.B. Pollack (1973). Mechanisms for Mars Dust Storms. *J. Atmos. Sci.*, 30, 749-762.

4. Sutton, J.L., Leovy, C.B., and J.E. Tillman (1978). Diurnal Variations of the Martian Surface Layer Meteorological Parameters During the First 45 Sols at Two Viking Lander Sites. *J. Atmos. Sci.*, 35, 2346-2355.

FIGURE 1. Model predictions of the diurnal variation of the friction velocity at the Viking lander 1 site during early summer for three different values of the dust optical depth. The friction velocity is proportional to the square root of the surface stress.



**THE NORTH POLAR SAND SEAS: PRELIMINARY ESTIMATES OF SEDIMENT VOLUME;** N. Lancaster and R. Greeley, *Department of Geology, Arizona State University, Tempe, Arizona 85287-1404.*

The North Polar region of Mars contains major accumulations of aeolian sediment in the form of extensive sand seas and dunefields (Breed et al., 1979; Tsoar et al., 1979). An estimate of the volume of sediment contained in the sand seas is necessary in order to assess their role in the martian sedimentary cycle. Spatial variations in sediment volume may provide information on the ways in which the sand seas have accumulated, and suggest possible origins and sediment sources. In this abstract we provide a preliminary estimate of dune sediment volume based on studies of dune morphometry.

The approach used combines data from terrestrial analogs of martian dunes with detailed mapping of dune morphometry (dune spacing, cover) from Viking Orbiter images. Studies of dunes in terrestrial sand seas have shown that dune cross-sectional area increases exponentially with dune height, whereas dune height increases linearly with dune spacing (Lancaster, 1988). Therefore areas of large dunes, although widely spaced, represent a net accumulation of sediment. The sediment thickness represented by the dunes is given by their equivalent, or spread-out, sediment thickness (EST). The relation between EST and dune spacing for terrestrial dunes (Fig.1) provides the means to derive estimates of sediment thickness from a parameter (dune spacing) that is relatively easily measured on orbital images. In many areas, dunes do not completely cover the surface, so estimates of sediment thickness need to be reduced in proportion to the area covered by dunes. These estimates of sediment thickness should be considered as minimum values; they are estimates of the sediment contained in the dunes, and do not take into account sediment that has accumulated below the dunes.

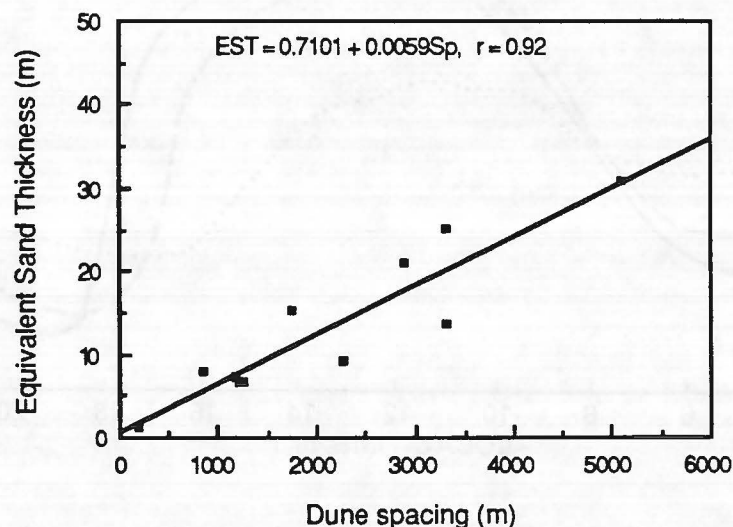


Fig.1. Relation between EST and dune spacing derived from terrestrial dunes.

Average dune spacing, and the percentage cover of dunes were measured on Viking Orbiter images of the North Polar region of Mars ( $> 70^\circ \text{N.}$ ). Calculations of EST were derived from these measurements and the relation in Fig.1., and mapped at a scale of 1:5m. (Fig. 3). Four major sand seas can be identified (Table 1), similar to those mapped by Tsoar et al. (1979) and Dial (1984). Within each sand sea, the area covered by dunes ranges from less than 5% to complete cover, with a mean cover of 50.7%. Dune spacing in the sand sea ranges between 150 and 2955m, with a mean of 512 m (Fig 2). Most North Polar dunes have a crest-to-crest spacing of 300-650 m. Very widely spaced dunes ( $>900$  m) are mostly scattered barchans in marginal areas of the sand seas. Assuming that martian dunes are a similar shape to terrestrial dunes, most

are therefore 12 to 26 m high, based on relations between dune spacing and height for transverse dunes in a variety of sand seas (Lancaster, 1988).

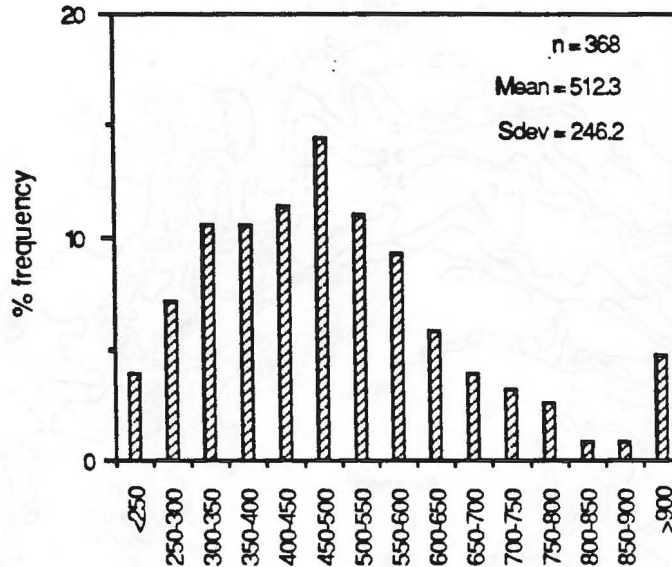


Fig. 2. Distribution of dune spacing (m) in the North Polar Sand Seas

Equivalent sediment thickness for the sand seas ranges from 0.10-0.50 m to a maximum of 5.0-6.0 m, with a mean of 1.81 m (Table 1; Fig. 3). EST is between 2 and 4 m over wide areas of the sand sea between 100 and 260° W. Average EST is greatest in this area, and significantly lower in the other dune areas. Within each sand sea, EST follows a consistent pattern, with the greatest sediment thickness in the center, decreasing toward the margins.

Table 1. Percentage cover of dunes, mean EST, and sediment volume in major North Polar sand seas

Latitude (°)	Longitude (°)	Area (km <sup>2</sup> )	Dune cover (%)	Mean EST (m)	Sediment volume (km <sup>3</sup> )
74-80	40-70	1.06 x 10 <sup>5</sup>	37.5	1.28	155.6
76-81	85-105	5.00 x 10 <sup>4</sup>	42.8	1.33	62.3
76-83	110-260	4.70 x 10 <sup>5</sup>	57.0	2.13	935.7
76-80	260-280	3.25 x 10 <sup>4</sup>	33.0	0.89	3.3

Sediment volumes (Table 1) were computed from the isopachs of sediment thickness (Fig. 3). The total volume of sediment contained in the dunes of sand seas of the North Polar region is 1195 km<sup>3</sup>, of which 78% lies in the large sand sea between 110 and 260° W.. This estimate is an order of magnitude less than that of Thomas (1982), but is based upon much more realistic views of the size of the majority of martian dunes, and the amount of sand they contain.

Our new estimate of dune sediment thickness tends to support hypotheses that the dune sands were derived from the Polar layered deposits (e.g. Breed et al, 1979; Thomas, 1982). There are clear relationships between eroding scarps and areas of dunes. Major areas of dunes, such as those between 40 and 70° W, lie downwind of major dissected areas of the perennial polar cap. It is perhaps significant that the major area of dunes between 110 and 260° W. lies between the present limits and large outliers of the perennial ice. Dissected areas of the polar cap and layered deposits extend for some 3.3 x 10<sup>5</sup> km<sup>2</sup> (Thomas, 1982). If the layered deposits

contained only 1% sand-sized material, some 275 m would have had to have been eroded to provide enough sediment to form the dunes. This is consistent with the local relief of 200-800 m noted by Blasius and Cutts (1982).

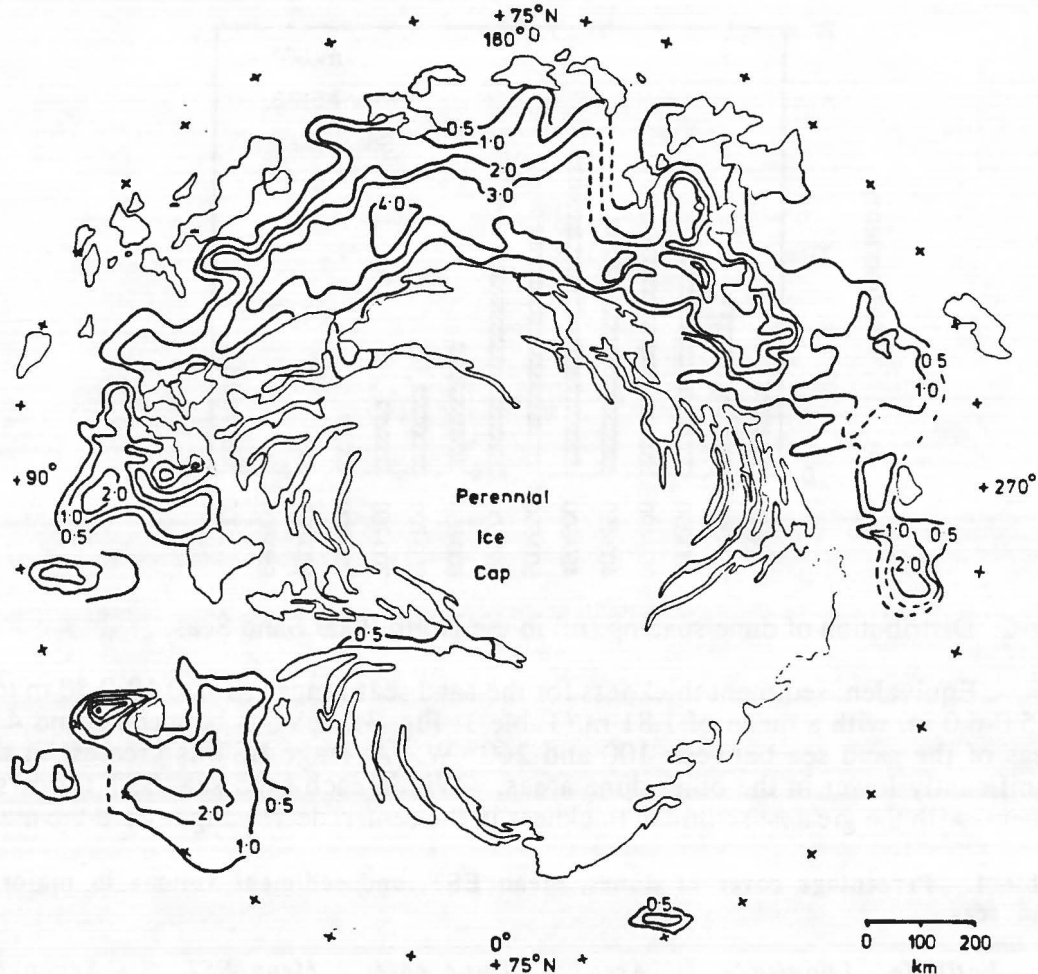


Fig. 3. Equivalent sediment thickness in the North Polar sand seas of Mars. Isopachs in meters.

### References

- Blasius, K.R., Cutts, J.A., and Howard, A.D., 1982. Topography and stratigraphy of Martian polar layered deposits. *Icarus*, 50: 140-160.
- Breed, C.S., Grolier, M.J. and McCauley, J.F. 1979. Morphology and Distribution of Common "Sand" Dunes on Mars: Comparison With the Earth. *Journal of Geophysical Research*. 84: 8183-8204.
- Dial, A.L., jr., 1984. *Geologic map of the Mare Boreum area of Mars*. U.S. Geological Survey Miscellaneous Investigations Series. Map 1-1640 (MC-1).
- Lancaster, N., 1988. The development of large aeolian bedforms. *Sedimentary Geology*, 55: 69-90.
- Thomas, P. 1982. Present wind activity on Mars: relation to large latitudinally zoned sediment deposits. *Journal of Geophysical Research*. 87: 9999-10,008.
- Tsoar, M., Greeley, R. and Peterfreund, A.R. 1979. Mars: the North Polar Sand Sea and Related Wind Patterns. *Journal of Geophysical Research*. 84: 8167-8180.

**VIKING PHOTOMETRIC AND ALBEDO STUDIES OF REGIONAL DUST TRANSPORT ON MARS; S.W. Lee and R.T. Clancy, Laboratory for Atmospheric and Space Physics, University of Colorado, Boulder, CO 80309**

There is abundant evidence that, at present, aeolian processes are active over much of the surface of Mars (cf. 1; 2). Previous studies have demonstrated that variations in regional albedo and wind streak patterns are indicative of sediment transport through a region (3; 4), while thermal inertia data [derived from the Viking Infrared Thermal Mapper (IRTM) data set] are indicative of the degree of surface mantling by dust deposits (5; 6; 7; 8; 9). The visual and thermal data are therefore diagnostic of whether net erosion or deposition of dust-storm fallout is taking place currently and whether such processes have been active in a region over the long term.

One of the consequences of variations in regional sedimentation patterns should be relative differences in surface texture and macroscopic roughness from region to region; photometric analysis of the visual brightness of a surface viewed under a variety of emission and phase angles may allow such differences to be quantitatively investigated (10; 11; 12). In addition, determination of regional photometric properties will place constraints on the interpretation of the related albedo and thermal data sets.

Disk-resolved (as opposed to disk-integrated) photometric studies of planetary surfaces from spacecraft are not common, and photometric studies of Mars using spacecraft data are rare indeed. Voyager images of Io have been used to investigate porosity and macroscale roughness of the surface (cf. 13; 14); these studies have indicated that it may be more appropriate to study relative regional differences in photometric properties, rather than to attempt physically rigorous modelling of the results. Images from the early Mariner missions were used to study a few selected regions (15); indications were that significant variations in surface properties were detectable. Only the first few months of Viking Orbiter IRTM data were systematically analyzed (5); again, significant variations in regional properties, as well as the effects of atmospheric aerosols, were detected.

During the course of the Viking missions, numerous IRTM observing sequences were designed with photometric analyses in mind. Several hundred emission-phase-function (EPF) sequences, in which the IRTM instrument observed the same area on the surface for an extended period as the spacecraft moved overhead, were obtained; of these, about 200 sequences were obtained during daytime. Typical sequences consist of several thousand to several tens of thousand individual measurements of surface brightness gathered over a wide range of emission and phase angles and with spatial resolutions of several tens of kilometers. In addition, about 100 sequences, scanning the whole disk of the planet from high altitude, were obtained at very low phase angles ( $< 20^\circ$ ). These observations were obtained randomly over much of the planet, but most lie within  $45^\circ$  of the equator. The IRTM data set, as a whole, is well calibrated, having been corrected for inter-spacecraft, inter-detector, and temporal calibration variations; a conservative estimate for the absolute uncertainty inherent in this data set is 1-2% (16). Thus, differences in regional properties inferred from photometric studies should be attributable to variations in the surface and/or atmospheric characteristics and not to calibration errors. To date, however, these sequences have not undergone the photometric analysis for which they were intended.

We are investigating the photometric properties of several regions on Mars through analysis of EPF and low-phase-angle IRTM observations. The results of these analyses, in conjunction with mapping of regional thermal properties (also from IRTM data) and temporal albedo variations (using IRTM and imaging data), are being used to infer details of regional sediment transport and consequent properties of the martian surface. The photometric study may also allow quantitative investigation of the properties of martian dust and aerosols. In addition to adding to our basic knowledge of the surface properties and geologic environment of the martian surface at present, these results, particularly those of the photometric analyses, should provide useful input for the design of observing sequences by various instruments aboard the Mars Observer spacecraft.

## REFERENCES

- 1) Veverka, J., P. Thomas, and R. Greeley (1977). A study of variable features on Mars during the Viking primary mission. *J. Geophys. Res.* 82, 4167-4187.
- 2) Thomas, P., J. Veverka, S. Lee, and A. Bloom (1981). Classification of wind streaks on Mars. *Icarus* 45, 124-153.
- 3) Lee, S.W., P.C. Thomas, and J. Veverka (1982). Wind streaks in Tharsis and Elysium: Implications for sediment transport by slope winds. *J. Geophys. Res.* 87, 10025-10042.
- 4) Lee, S.W. (1986). Regional sources and sinks of dust on Mars: Viking observations of Cerberus, Solis Planum, and Syrtis Major (abstract), In *Symposium on Mars: Evolution of its Climate and Atmosphere* (V. Baker et al., eds.), pp. 71-72, LPI Tech. Rpt. 87-01, Lunar and Planetary Institute, Houston.
- 5) Kieffer, H.H., T.Z. Martin, A.R. Peterfreund, B.M. Jakosky, E.D. Miner and F.D. Palluconi (1977). Thermal and albedo mapping of Mars during the Viking primary mission. *J. Geophys. Res.* 82, 4249-4295.
- 6) Christensen, P.R. (1982). Martian dust mantling and surface composition: Interpretation of thermophysical properties. *J. Geophys. Res.* 87, 9985-9998.
- 7) Christensen, P.R. (1986). Regional dust deposits on Mars: Physical properties, age, and history. *J. Geophys. Res.* 91, 3533-3545.
- 8) Christensen, P.R. (1986). The distribution of rocks on Mars. *Icarus* 68, 217-238.
- 9) Jakosky, B.M. (1986). On the thermal properties of martian fines. *Icarus* 66, 117-124.
- 10) Goguen, J.D. (1981). A theoretical and experimental investigation of the photometric functions of particulate surfaces. Ph.D. dissertation, Cornell University, Ithaca, N.Y.
- 11) Hapke, B. (1981). Bidirectional reflectance spectroscopy. 1. Theory. *J. Geophys. Res.* 86, 3039-3054.
- 12) Hapke, B. (1984). Bidirectional reflectance spectroscopy. 3. Correction for macroscopic roughness. *Icarus* 59, 41-59.
- 13) Clancy, R.T and G.E. Danielson (1981). High resolution albedo measurements on Io from Voyager 1. *J. Geophys. Res.* 86,, 8627-8634.
- 14) Simonelli, D.P, and J. Veverka (1986). Phase curves of materials on Io: Interpretations in terms of Hapke's function. Submitted to *Icarus*.
- 15) Young, A.T., and S.A. Collins (1971). Photometric properties of the Mariner cameras and of selected regions of Mars. *J. Geophys. Res.* 76, 432-436.
- 16) Pleskot, L.K., and E.D. Miner (1981). Time variability of martian bolometric albedo. *Icarus* 45, 179-201.

CORRELATIONS BETWEEN SURFACE ALBEDO FEATURES AND GLOBAL DUSTSTORMS ON MARS: L. J. Martin, Planetary Research Center, Lowell Observatory, Flagstaff, Az., and P. B. James, University of Missouri-St. Louis, St. Louis, Mo.

Seasonal and interannual variability of albedo features on Mars has been familiar to terrestrial astronomers for a long time (Slipher, 1962). The albedo history of the Solis Planum area during the Viking Mission has been investigated in detail by S. Lee (1986); the period includes the two major 1977 storms observed by the spacecraft. Solis Planum was a source for dust during southern spring and summer, when local dust clouds were frequently seen in the region, while sedimentation apparently replenished the region during the rest of the year. Thus the albedo behavior of dust sensitive regions is probably closely correlated with the global dust storm behavior in a particular year.

The two primary source areas for dust during the growth phases of major dust storms on Mars have historically been the Hellas and the Solis Planum regions (Briggs et al., 1979). Our 1986 observations showed that both of these areas were unusually dark, suggesting a reduced dust inventory in the areas where major storms tend to develop; in fact, most of the normally bright features in the southern hemisphere were darker than usual in 1986. No major dust storms developed between  $L_S=160^\circ$  and  $L_S=330^\circ$  in 1986, a period which includes all of the classic dust storm period on the planet; this supports the depletion of dust available in the source regions. During the 1984 opposition, which occurred at a somewhat earlier season, Hellas was bright and Solis Lacus was about average in size and albedo; however, other albedo features were already darker than usual. This suggests that the mechanisms working to deplete these areas, such as the local dust storms in the Solis Planum area, were active during 1984 but that there was insufficient replenishment from the northern hemisphere to sustain substantial dust activity in 1986.

During most years Hellas can be identified as a large, circular area which is one of the brightest features on the planet, comparable to the polar caps and the bright areas, such as Arabia, in the northern hemisphere. Hellas was distinctly bright in the dust storm years of 1956, 1971, and 1973; but Hellas was no brighter than its surroundings on most 1986 images, making its identification difficult. Solis Lacus is normally a dark feature surrounded by lighter areas (Thaumasia, Syria, and Sinai); in 1986 Solis Lacus was very dark and larger than it had been since 1926. It covered much of the adjacent

areas which themselves appeared less bright than in normal years. Most of the southern hemisphere, particularly between latitudes  $-30^{\circ}$  and  $-60^{\circ}$ , was darker than usual in 1986; the only exceptions were the Ausonia and Eridania regions just to the east of Hellas. The behavior of the albedo features in the southern hemisphere during the 1986 apparition is the exception to the "rule" proposed by Slipher (1962) and others that such areas remained light through southern spring and darkened in summer and implies that dust inventories were below normal for most of the southern hemisphere in 1986. Thus the dust clouds reported in Hellas by some observers (D. Parker, private communication) may not have been able to expand into major storms due to a lack of dust.

If the very dark aspect of the southern hemisphere and the relatively clear 1986 dust storm season do imply a significant depletion of dust in the source regions, it seems likely that mechanisms must exist to return dust from sinks in the northern hemisphere; these mechanisms are less well documented than the perihelic duststorms which originate in the southern hemisphere. One might speculate that we saw in 1986 an extremum in a dust cycle having a period of several Mars years. The 1988 apparition, which spans another dust storm season, will give us an opportunity to further investigate the development of these albedo features and their effects on dust storm activity.

Briggs, G., W. Baum, and J. Barnes (1979). *J. Geophys. Res.* 84, 2795-2820.

Lee, S. (1986). LPI Technical Report Number 86-09, 44-45.

Slipher, E. (1962). *Mars: The Photographic Story*, Northland Press, Flagstaff, Az.

EARTHBASED MONITORING OF THE MARTIAN ATMOSPHERE DUST OPACITY;  
T.Z. Martin, Jet Propulsion Laboratory

The dust content of the Mars atmosphere is known to exhibit considerable interannual variability; specifically, major dust storms occur in some years but not others. The effect of dust on geologic processes, deposition of polar volatiles, atmosphere dynamics, and remote sensing observations makes it important to understand this variability. Recent theoretical work on the subject (1) has emphasized the need for more data.

Monitoring of dust behavior on Mars has been sporadic since the failure of the Viking 1 lander in 1982. Visual photography once performed systematically by the Planetary Patrol has been discontinued. However, even when operating they acquired data only when Mars exceeded 13 arc sec in diameter - just 20% of the time. Historically, few dust storm seasons have been observed from earth or by spacecraft.

Mars is rarely near opposition during the prime dust storm season (Ls 200-300). However, that circumstance obtained in 1986 and 1988. The author undertook in 1986 to begin earthbased monitoring of Mars' dust opacity in the thermal infrared (2). This work followed naturally the analysis performed on the Viking IR Thermal Mapper data to extract opacity information.

The silicate dust band used in the IRTM work (3) falls in the 10 micrometer window of the earth's atmosphere. Observations in this region are unaffected by scattered sunlight, so Mars may be observed in the daytime far from opposition. Mars is never less than 4 arc sec in diameter, and therefore in principle at least hemispherical differences in opacity can be established with mapping performed with a 2 second aperture.

The NASA IR Telescope Facility at Mauna Kea was chosen for its IR transparency, excellent tracking and pointing (needed to find stars in the daytime), data acquisition software, and especially the facility detector system: a SiAs photoconductor coupled with a circular variable filter spectrometer covering 6.5-13 micrometers with 1% spectral resolution. The silicate band is well resolved without wasting signal, and the terrestrial ozone band, also at 9.6 micrometers, can be discriminated. A comparison between the appearance of the earthbased spectrum and data from the 1969 Mariner 7 IR Spectrometer is shown in Fig. 1.

Derivation of opacity information from the behavior of the silicate band rests on the assumption that the dust-bearing atmosphere of Mars during the daytime is normally cooler than the surface; the lapse rate is about 4K/km under clear conditions and about 2K/km when dust content is high. In these conditions a silicate absorption appears, whose depth is proportional to the dust abundance. While an independent measure of the atmospheric temperature would be valuable, such as could be determined from the 15 micrometer CO<sub>2</sub> band, the silicate band behavior alone provides a good measure of the changes in opacity. The 15 micrometer band

is inaccessible due to the overlapping telluric feature.

We obtain images of Mars in five wavelengths: 7.8, 8.9, 9.5, 10.4, and 12.0 micrometers. The first and last of these are "continuum" measurements, and the other three fall within the silicate band. Conversion to brightness temperature is done using observations of standard K type stars lacking silicate shells. From the set of images we form a single "band depth" image based on the relative band strength as observed in Mariner 9 IRIS spectra. Although absolute calibration of the Mars images is a goal, the band depth does not depend strongly on the derived absolute temperature.

Successful measurements have been obtained on ten out of ten observing runs completed to date (2-3 half nights each). The seasonal coverage is shown in Table 1.

At this writing, no NASA funding has been obtained specifically for acquisition or analysis of these data; travel support in 1988 was provided by The Planetary Society. Reduction of the 750 Mars images proceeds slowly. However, detailed analysis of several data sets has been done to support proposals. We show in Fig. 2 a single 12.0 micrometer image from April 1988, and the corresponding "band depth" image derived using data at all 5 wavelengths. The consistency of these derived images, which carry model-independent information related to the dust opacity, is good evidence that the technique is working. Derivation of dust opacity will require assumptions about the emission angle dependence of the absorption, the temperature profile, and the surface emissivity.

The author performed this work as a visiting astronomer at the Infrared Telescope Facility, which is operated by the University of Hawaii under contract to the National Aeronautics and Space Administration.

1. Haberle, R.M. (1986) Science vol. 234, p. 459.
2. Martin, T.Z. (1986) Bulletin of the AAS vol. 18, p. 806.
3. Martin, T.Z. (1986) Icarus vol. 66, p. 2.

Table 1

## Seasonal Coverage

Date	Ls	Date	Ls
1986 Jul 2-4	198	1988 Feb 11-13	144
Aug 6-7	219	Mar 21-23	165
Sep 30-31	253	Apr 14-16	178
Nov 14-15	282	Jun 21-22	218
		Jul 29-31	242
1987 Feb 9-10	333	Aug 31-32	263
Mar 3-4	345	Sep 8-9	268
		Dec 9-10	323

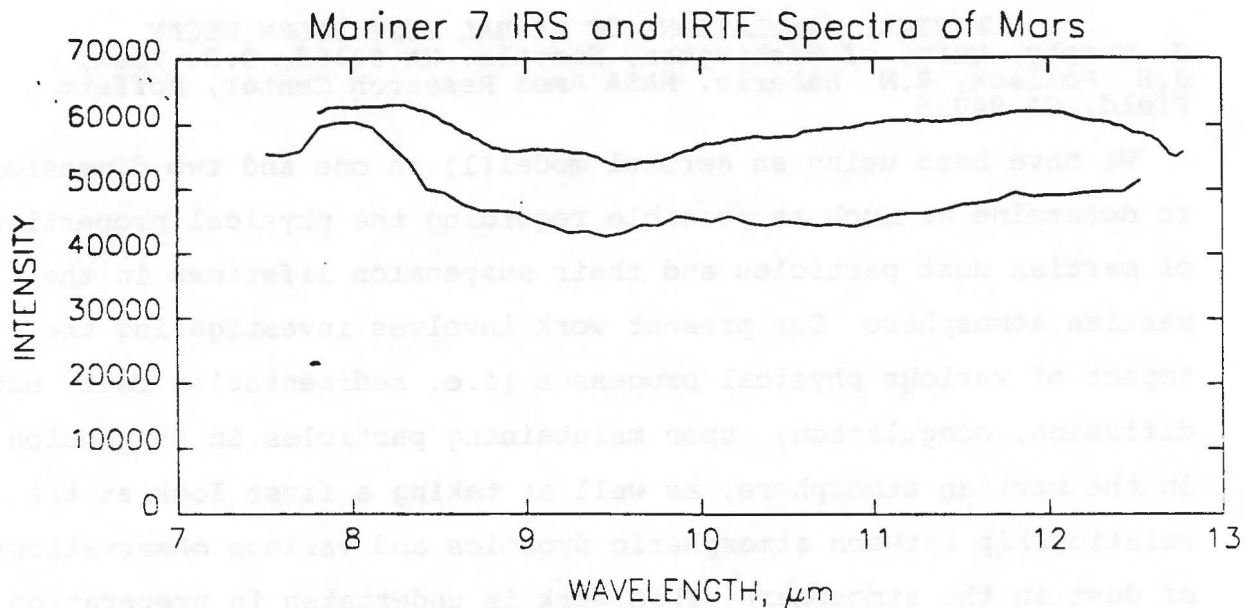


Fig. 1. Spectra of the silicate band region obtained by the Mariner 7 IR spectrometer (top) in 1969 and from the IRTF on June 23, 1988. The IRS spectrum has been corrected for instrumental response. The IRTF spectrum is ratioed to that of Beta And; a correction for the difference in slope between a 300 and 2700K blackbody has also been applied.

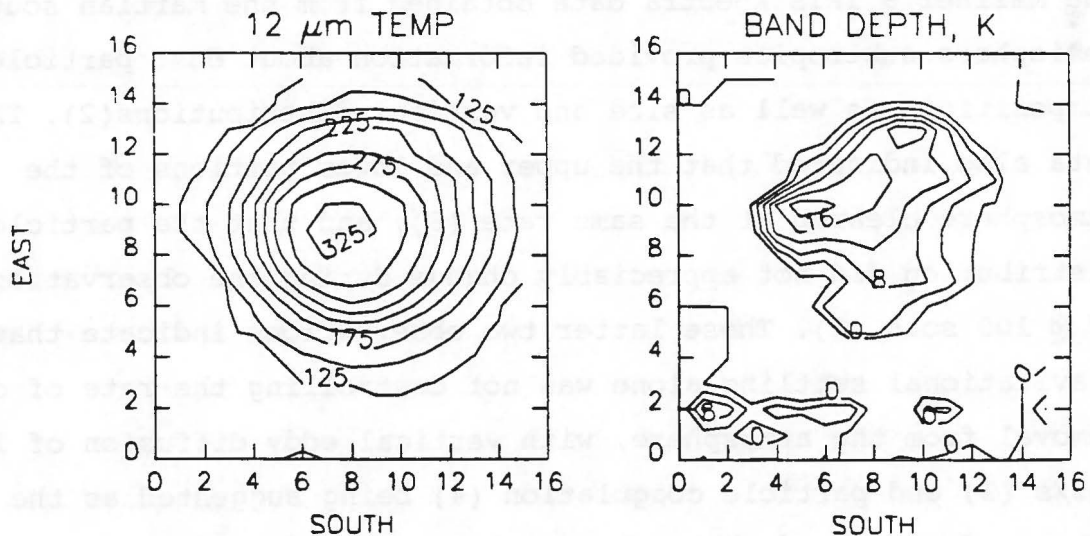


Fig. 2. Brightness temperature image of Mars, April 17, 1988 1810 UTC, and the corresponding silicate band depth image derived from images at 7.8, 8.9, 9.5, 10.4, and 12.0 micrometers.

NUMERICAL SIMULATIONS OF GLOBAL DUST STORM DECAY  
J. Murphy, Univ. of Washington, Seattle, WA 98195, O.B. Toon,  
J.B. Pollack, R.M. Haberle, NASA Ames Research Center, Moffett  
Field, CA 94035

We have been using an aerosol model(1) in one and two dimensions to determine as much as possible regarding the physical properties of martian dust particles and their suspension lifetimes in the martian atmosphere. Our present work involves investigating the impact of various physical processes (i.e. sedimentation rate, eddy diffusion, coagulation) upon maintaining particles in suspension in the martian atmosphere, as well as taking a first look at the relationship between atmospheric dynamics and various observations of dust in the atmosphere. This work is undertaken in preparation for the coupling of the aerosol model and the NASA Ames Mars GCM to simulate the atmospheric circulation and dust transport during a global dust storm.

Martian global dust storm decay phases have been observed by Mariner 9 (1971) and the Viking landers and orbiters (1977a,1977b). The Mariner 9 IRIS spectra data obtained from the martian southern hemisphere subtropics provided information about dust particle composition, as well as size and vertical distributions(2). These data also indicated that the upper and lower portions of the atmosphere cleared at the same rate (3), and that the particle size distribution did not appreciably change during the observation time of @ 100 sols (2). These latter two observations indicate that gravitational settling alone was not controlling the rate of dust removal from the atmosphere, with vertical eddy diffusion of  $1.E+07$   $cm^2/s$  (3) and particle coagulation (4) being suggested as the reasons for each of these observations, respectively.

The visible optical depth values provided by the Viking lander imaging experiment (at 23 N latitude), in conjunction with the dust particle properties inferred from the Mariner 9 IRIS data, give us the opportunity to investigate the importance of the previously

NUMERICAL SIMULATIONS OF GLOBAL DUST STORM DECAY  
J. Murphy, O. B. Toon, J. B. Pollack, R. M. Haberle

mentioned physical processes as they relate to a global dust storm decay. With a 1-D version of the aerosol model we have studied the impact of these physical processes by reproducing the optical depth declines observed at Viking lander 1 during the 1977a & 1977b dust storm decay phases. The aerosol model contains the previously mentioned physically important processes for dust suspension maintenance, and by varying their magnitude and/or inclusion in our simulations, we arrived at a combination of these factors which produced the best fit to the data. For initial conditions we chose particle size distribution # 1 from (2), constant mass mixing ratio with height (3), dust composed of montmorillonite 219b (2), and a static, isothermal atmosphere at 220K.

The 1977a storm peak optical depth at lander 1 was @ 3.2 (5,6), decreasing exponentially with a time constant of 75 sols initially, and more slowly after 75 sols. In our simulations, spherical dust particles fell out much too quickly, even in the presence of strong diffusion ( $1.E+07$  cm<sup>2</sup>/s), to reproduce the observations. Increased diffusion and vertical variation of the diffusion had negligible additional effect, while the inclusion of Brownian coagulation resulted in slightly more rapid optical depth declines. Coagulation did little to quench the greater loss of large particles relative to the smaller particles. As a means of reducing the Stokes-Cunningham determined particle fall speeds, the particle shape was varied, increasing the surface area to volume ratio thereby reducing the fall speeds. Disc shaped particles with a thickness to diameter ratio of 0.1, in the presence of vertical diffusion  $1.E+07$  cm<sup>2</sup>/s, resulted in an optical depth decline consistent with the lander 1 observations of the 1977a storm. Such plate-like particles are not inconsistent with those expected for clay particles, and also agree with the particle shape results from lander 1 imaging (5).

The 1977b storm, with a peak VL1 optical depth of @ 6.0 (6), had

NUMERICAL SIMULATIONS OF GLOBAL DUST STORM DECAY  
J. Murphy, O.B. Toon, J.B. Pollack, R.M. Haberle

an initial exponential decay rate 33% more rapid than the 1977a event. This rapid decay rate was best simulated with disc shaped particles (thickness/diameter=0.15) which were a bit "fatter" than those of the 1977a storm best fit, and a vertical eddy diffusion value of  $1.E+05$  cm<sup>2</sup>/s.

This discrepancy between particle shape (and diffusion) for the two storms is likely not explained by different particle shapes (nor necessarily different diffusion coefficients) for each storm, rather we are now investigating a new idea. This idea is that dynamics controls the local decay rate of the dust storms by the resupply of dust and by vertical velocities that are of the same order as the fall velocities. We are in the process of analyzing these processes using a 2-D configuration of the aerosol model and a 2-D wind field produced by the dynamical model of (7). This dynamical model can be run under conditions of varying optical depth to produce cross equatorial Hadley type circulations which are representative of the atmospheric flow during a global dust storm.

As well as helping to more clearly define the particle shape appropriate for use in 3-D dust storm simulations, we anticipate that our 2-D investigations will shed some light upon whether the lack of particle size distribution change inferred from Mariner 9 IRIS data is site specific (i.e. in the dust source region and/or the region of upward vertical motion) or a more global phenomenon.

REFERENCES

1. Toon, O.B., Turco, R.P., Westphal, D., Malone, R., and M.S. Liu, submitted to JAS, in press 1988
2. Toon, O.B., Pollack, J.B., and C. Sagan, ICARUS, 30, 663-696, 1977
3. Conrath, B.J., ICARUS, 24, 36-46, 1975
4. Rossow, W.B., ICARUS, 36, 1-50, 1978
5. Pollack, J.B., Colburn, D.S., Flasar, F.M., Kahn, R., Carlston, C.E., and D. Pidek, JGR, 84, 2929-2945, 1979
6. Zurek, R.W., ICARUS, 45, 202-215, 1981
7. Haberle, R.M., Leovy, C.B., and J.B. Pollack, ICARUS, 50, 322-368, 1982

SIMULATIONS OF THE GENERAL CIRCULATION OF THE MARTIAN ATMOSPHERE  
II. DUST STORMS; J.B. Pollack, R.M. Haberle, NASA Ames Research Center, and  
J. Schaeffer, H. Lee, Sterling Software

We have conducted numerical simulations of the general circulation of the Martian atmosphere with a 3 dimensional model based on the primitive equations of meteorology. Line by line calculations were carried out to obtain an accurate specification of the absorption properties of carbon dioxide gas at solar and thermal wavelengths and single and multiple scattering calculations were performed to derive an accurate specification of the interactions of suspended dust with solar and thermal radiation. A bulk parameterization scheme was used to evaluate the exchange of heat and momentum between the surface and the atmosphere. The model incorporated Mars consortium information on the spatially varying topography, thermal inertia, and albedo of the surface.

A large number (16) of numerical experiments were carried out for spatially and temporally constant dust loading (for a given experiment) to determine the steady state response of the atmosphere to different choices of dust optical depth (0-5) and seasonal date (6 dates spaced about  $60^\circ$  of  $L_s$  apart). In all cases, a uniform horizontal grid of  $7\frac{1}{2}^\circ$  of latitude by  $9^\circ$  of longitude was used and 13 vertical levels spanning an altitude range of 47 km was employed.

These simulations have a number of implications for dust storm genesis, dust transport, and dust removal. Factors that influence the magnitude of the surface wind stress and therefore the ability to initiate the saltation of sand and the suspension of micron sized dust include seasonal date, the dust optical depth, topographical and thermal inertia gradients, and polar cap boundaries. Large surface wind stresses occur when Mars is close to perihelion, at times of enhanced dust loading, in association with baroclinic wave activity in the winter hemisphere, and in association with certain types of topographical slopes at low latitudes.

Various components of the circulation respond in different ways to enhanced levels of atmospheric dust, thereby influencing both the rate and degree of dust spreading from localized sources. For example, both the strength and extent of the Hadley circulation are enhanced as the dust loading increases.

Carbon dioxide condenses in the atmosphere as well as on the surface in the winter polar regions. Condensation is likely to take place on suspended dust particles and thereby help to remove dust in the winter polar region.

**INFRARED TRANSMISSION MEASUREMENTS OF MARTIAN SOIL ANALOGS;** Ted L. Roush, NASA Ames Research Center, M/S 245-3, Moffett Field, CA 94035

Infrared spectra, in the 2.5 to 25 $\mu\text{m}$  wavelength region (4000-400  $\text{cm}^{-1}$ ), of silicate minerals typically exhibit strong absorption features located near 10- and 20  $\mu\text{m}$  due to the stretching and bending modes, respectively, of the  $\text{SiO}_4$  tetrahedra (1,2). The complexity and wavelength position of these absorptions are used to identify the silicates according to structural classes (eg. ortho- versus phyllosilicates), as well as, specifying its proper position within an isomorphous series (1,2).

Spectroscopic observations of Mars, beyond 5 $\mu\text{m}$  which include continuous wavelength coverage, are limited to data collected by the Mariner 6, 7, and 9 spacecraft. The first two of these missions were fly-bys and covered the  $\sim$ 1.9-14.5 $\mu\text{m}$  wavelength region (3), while the third was an orbiter and covered the 5-50 $\mu\text{m}$  wavelength region (4). In each of these data sets there is a strong silicate signature near 10 $\mu\text{m}$  (5,6,7,8). When Mariner 9 arrived at Mars the entire planet was engulfed by a dust storm which slowly cleared with time (7). Since the dust particles were suspended, this situation provided an excellent opportunity for the comparison of the martian data to transmission measurements of candidate surface materials (7). The wavelength position of the 10  $\mu\text{m}$  silicate band has been used to indicate the presence of material of basic to intermediate composition (5,6), as well as, some limited clay compositions (6,7). Figure 1 illustrates brightness temperature spectra from the Mariner 9 data and the 10 $\mu\text{m}$  (1000  $\text{cm}^{-1}$ ) band is quite obvious. The Mariner 9 data also exhibit an additional strong silicate signature near 20 $\mu\text{m}$  (400-500  $\text{cm}^{-1}$ ) (7). Previous interpretation of the 10 and 20 $\mu\text{m}$  bands seen in the Mariner 9 data are most consistent with the mineral montmorillonite but some discrepancies remain (7). In particular, the 20 $\mu\text{m}$  band observed in the martian data exhibit a broad spectral shape which is inconsistent with a high degree of silicate polymerization associated with clay minerals (7), and the relative band intensities observed in the martian data (10 $\mu\text{m}$  band > 20 $\mu\text{m}$  band) is inconsistent with the montmorillonite previously used for comparison purposes (9).

Subsequent to the Mariner 9 mission, comparisons of the 0.35-2.5 $\mu\text{m}$  earth-based telescopic observations of Mars with laboratory reflectance spectra measured for a variety of candidate martian surface materials have resulted in the interpretation that the bright regions and soils of Mars are composed chiefly of amorphous (10,11,12)  $\text{Fe}^{3+}$ -bearing materials. In the visible and near-infrared (0.35-2.5 $\mu\text{m}$ ), terrestrial palagonites provide one example of spectral analogs for martian surface materials (10,11,12). In the 0.35-2.0 $\mu\text{m}$  wavelength region, spectral measurements of iron-substituted smectites provide another possible spectral analog (13), however beyond 2.0 $\mu\text{m}$  their spectra exhibit crystalline clay absorption features which are poorly defined in the observed martian spectra (12). The presence of the poorly defined clay bands in the martian spectra has been interpreted as an indication that the bright regions and soils on Mars are either slightly more crystalline than the terrestrial palagonites, or alternatively, they contain minor amounts of Mg-bearing crystalline clays admixed with the palagonites (12).

To my knowledge, there have been no previous comparisons of the spectral properties of amorphous palagonites at the wavelengths which were covered by the Mariner 9 data. Additionally, another useful comparison to the Mariner 9 data would include the spectral properties of a variety of smectite minerals. An investigation was undertaken to measure the transmission properties of palagonites, as well as, several smectite minerals. While the optical constants, necessary for a quantitative comparison to the Mariner 9 data, remain to

be derived for these materials, results of the initial transmission measurements are presented here and a qualitative comparison to the Mariner 9 data is made.

Milligram amounts of samples were mixed with KBr powder and then pressed into a coherent pellet using approximately 10 tons of pressure. Spectra of the pressed pellets were obtained, in the 2.5 to 25  $\mu\text{m}$  wavelength region, using a Nicolet 7199 Fourier Transform Spectrometer. Each spectrum presented was obtained at a spectral resolution of 4  $\text{cm}^{-1}$ , which remained constant at all wavelengths, and consists of 100 individual spectra which were coadded to improve signal-to-noise. Spectra presented here were corrected to the same measurement conditions but with no sample in the instrument beam.

Figure 2 shows the spectra of the smectite minerals in the 1800-400  $\text{cm}^{-1}$  region. The spectra of these samples all exhibit strong absorptions, near 1000 and 400-500  $\text{cm}^{-1}$  (10- and 20-25  $\mu\text{m}$ ), which are due to the silicate fundamentals. A qualitative comparison to Figure 1 illustrates that while in some cases the 10  $\mu\text{m}$  band positions and relative intensities of the 10- and 20  $\mu\text{m}$  spectra of the smectites provide a close comparison to the Mariner 9 data, the spectra are generally too complex in the 20  $\mu\text{m}$  region to remain consistent with the spacecraft data.

As seen in Figure 3, the spectra of the two palagonites also exhibit absorptions which are centered near 1000 and 400-500  $\text{cm}^{-1}$  due to the silicate fundamentals. Qualitative comparison of both palagonite spectra to the Mariner 9 data of Figure 1 shows that the 10  $\mu\text{m}$  band position, the relative intensities of the 10 and 20  $\mu\text{m}$  bands and the relative widths of the 20  $\mu\text{m}$  bands provide a close analog to the Mariner 9 data. However, while the spectra of both palagonites provide a better comparison to the Mariner 9 data near 20  $\mu\text{m}$  than the smectites, they still exhibit more complex structure than that seen in the Mariner 9 data.

In summary, based on silicate absorption band position, relative band intensity, and 20  $\mu\text{m}$  band shape and complexity, the 2.5 to 25  $\mu\text{m}$  transmission spectra of two palagonites qualitatively provide a better comparison to Mariner 9 data than the spectra of the four smectites studied here. However, even the palagonites spectra exhibit a complexity near 20  $\mu\text{m}$  which is not seen in the Mariner 9 data.

**ACKNOWLEDGEMENTS:** This research is supported by the National Research Council. I would like to thank Lou Allamandola and Scott Sandford for use of their spectrometer, Ted Bunch for use of his laboratory facility, and James Pollack for his continued encouragement.

**REFERENCES:** (1)Gadsden, J.A. (1975) *Infrared Spectra of Minerals and Related Compounds*, Butterworths. (2)Farmer, V.C., (1974) In *The Infrared Spectra of Minerals*, Mineralogical Society, Monograph 4, Mineralogical Society, London, 539pp. (3)Herr, K.C., P.B. Forney, and G.C. Pimentel (1972) *Appl. Opt.*, 11, 493-501. (4)Hanel, R.A., B. Schlachman, E. Breihan, R. Bywaters, F. Chapman, M. Rhodes, D. Rodgers, and D. Vanous (1972) *Appl. Opt.*, 11, 2625-2634. (5)Hanel, R., B. Conrath, W. Hovis, V Kunde, P. Lowman, W. Maguire, J. Pearl, J. Pirraglia, C. Prabhakara, B. Schlachman, G. Levin, P. Straat, and T. Burke (1972) *Icarus*, 17, 423-442. (6)Hunt, G.R., L.M. Logan, and J.W. Salisbury (1973) *Icarus*, 18, 459-469. (7)Toon, O.B., J.B. Pollack, and C. Sagan (1977) *Icarus*, 30, 663-669. (8)T.Z. Martin, 1988, *personal communication*. (9)O.B. Toon (1987) *personal communication*. (10) Evans, D.L. and J.B. Adams (1980) *Proc. Lunar Planet. Sci. Conf. 11th*, 757-763. (11)Singer, R.B. (1982) *J. Geophys. Res.*, 87, 10159-10168. (12)Singer, R.B. (1985) *Adv. Space Res.*, 5, 59-68. (13)Banin, A., G.C. Carle, S. Chang, L.M. Coyne, J.B. Orenberg, and T.W. Scattergood (1988), In *Origins of Life*, in press. (14)Bruckenthal, E.A. (1987) *M.S. thesis, Univ. Hawaii* (15)Roush, T.L. (1987) *Ph.D. dissertation, Univ. Hawaii*

Figure 1. Mariner 9 spectra of orbit 56 (top) and orbit 8 (bottom), adapted from (7). The gap between 650 and 800  $cm^{-1}$  is due to martian atmospheric  $CO_2$  absorption. The broad absorptions near 500 and 1000  $cm^{-1}$  correspond to the silicate tetrahedral bending and stretching fundamentals, respectively.

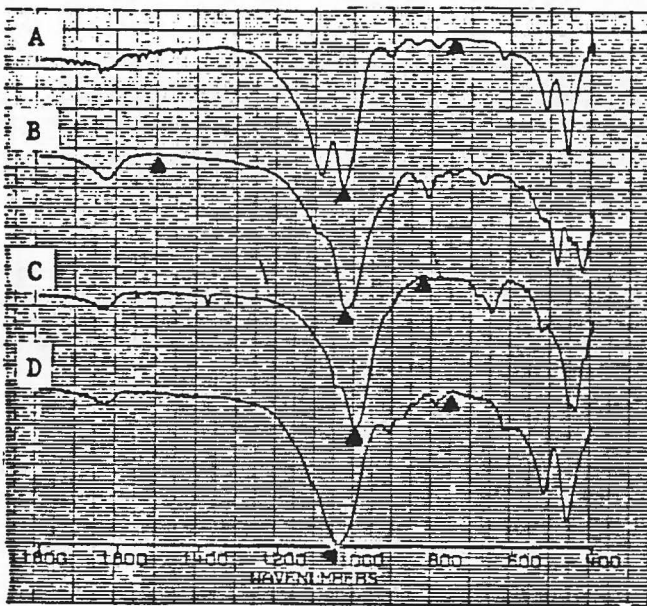
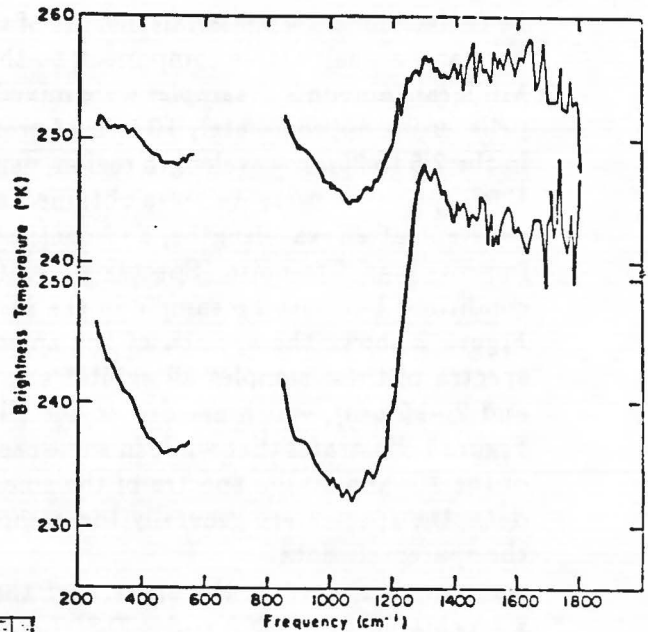
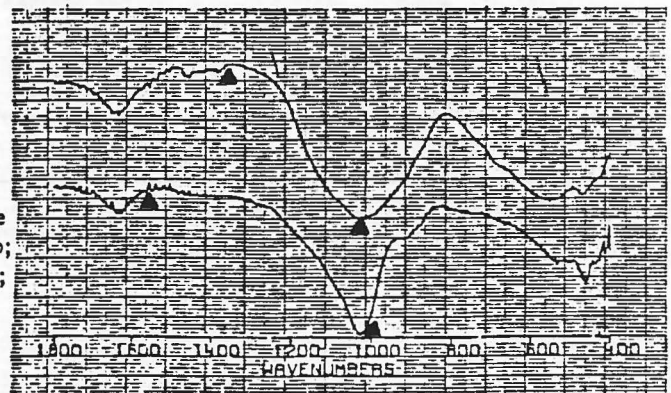


Figure 2. Transmission spectra of smectite minerals, minimum and maximum values of transmission are indicated on each curve. Curve A is Ca-Montmorillonite (14) (min=57.3, max=84.1). Curve B is nontronite, the ferric montmorillonite (15) (min=40.0, max=87.8). Curve C is saponite, the Mg equivalent of montmorillonite (14) (min=35.0, max=77.7). Curve D is Na-montmorillonite (15), (min=16.7, max=81.8).

Figure 3. Transmission spectra of palagonites, the weathering products of basaltic glass, VOL15 (15) (top; min=48.0, max=84.2) and Pahala Ash (14) (bottom; min=48.4, max=75.5).



**DUST IN THE POLAR REGIONS OF MARS: IS IT THE SAME AS AT LOW LATITUDES? P. C. Thomas, CRSR, Cornell University, Ithaca, NY**

Color and albedo information suggest that some of the northern polar layered deposits are similar to the bright areas of Arabia Terra. However, a dark component in the polar deposits complicates this interpretation. The mobile component(s) of low latitude variable features is being compared to that involved in north and south polar wind streaks. Any significant differences in the polar and equatorial dust are important in interpreting the global dust budget.

## DEPOLARIZED RADAR ECHOES AND DUST ON MARS

T. W. Thompson, Jet Propulsion Laboratory, Pasadena, CA 91109  
H. J. Moore, U.S. Geological Survey, Menlo Park, CA 94025

We have modeled depolarized echoes of 12.5-cm radio transmissions backscattered from Mars. The model (1) reproduces the variations of the total radar cross sections with longitude observed by the Goldstone radar in 1986 along 7°S (fig. 1); (2) yields larger magnitudes of total radar cross section along 22°N than those along 7°S -- in accordance with the 1980-1982 Arecibo observations (fig. 1); and (3) produces depolarized echo spectra that broadly match those observed by Arecibo (fig. 2). In the observations, both polarized and depolarized echoes from continuous wave radio transmissions were received and sampled as Doppler-spread spectra (1,2,3,4,5).

In our model, Martian depolarized echoes behave like lunar depolarized echoes from the maria, terrae, and young craters. Thus, Martian depolarized echo strengths per unit projected area are constant, but echo strengths vary from region to region. We divided the surface of Mars into sixty-one regions composed of 1°x 1° arrays which are called radar map units. These radar map units were defined by, first, generalized geologic map units (6,7,8) and, second, thermal inertia map units (9,10,11). Depolarized echo strengths were then assigned to the radar map units and tested against the observations using a "trial and error" method. In the "trial and error" method, the goal was to adjust the model echo strengths of the sixty-one radar map units until the model (1) matched the magnitudes of the Goldstone radar cross sections at all longitudes, (2) produced larger cross sections in the Tharsis region at 22°N than at 7°S, and (3) produced depolarized echo spectra that broadly matched those observed by Arecibo.

Model depolarized cross sections of the radar map units vary from 0.007 to 0.175. Cross sections for cratered uplands and other old terrains are 0.010, but those for the northern plains range from 0.015 to 0.040. Young volcanoes have cross sections that range from 0.070 to 0.175 and those of their surrounding lava plains range from 0.050 to 0.160. These cross sections are larger than that expected for the Moon (about 0.005) at the same wavelength (1); the cross section of the near rim flank the crater Tycho should be near 0.07.

Depolarized echoes are produced by wavelength-size (0.04-0.4 m) roughness elements at or near the surface and their strengths are related to the concentrations of the roughness elements, their depth below the surface, and the electrical properties of the matrix containing the buried roughness elements (12,13). A semi-quantitative interpretation of the echoes (14,5) implies that the concentrations of roughness elements such as slags and blocks on lava flows or rocks range from 3 to 76%.

Large model depolarized echo strengths (0.05 to 0.160) and inferred concentrations of roughness elements (22 to 70%) are associated with the lava plains of the Tharsis, Amazonis, and Elysium regions where thermal inertias are so low that loose dust is required at the surface (9,10,11). Only a few centimeters of loose dust are required to produce these low thermal inertias

(15) and radar backscatter would be unaffected by such thin layers. On the other hand, the low normal reflectivities of quasi-specular echoes ( $0.041 \pm 0.015$ ) from these regions (1,2), experimental data (16,17), and theory (18) imply the presence of substantial thicknesses of low density materials (about  $1,100 \pm 200 \text{ kg/m}^3$ ) with relative dielectric constants near  $2.3 \pm 0.4$ . If the low density materials are entirely dusts, local thicknesses of the dusts must be at least 3 to 7 m, but only 30 to 78% of the areas need be covered by the thick dust deposits.

Arabia is another region associated with low thermal inertias (9,10,11) which again implies that the uppermost few centimeters of materials are loose dusts. Here, the model depolarized echo strength (0.008) implies a concentration of roughness elements of about 3%; these roughness elements are probably rocks because lava flows are rare. In contrast with the Tharsis region, the normal reflectivity ( $0.061 \pm 0.015$ ) for Arabia (1), experimental data (16,17), and theory (18) imply that moderately dense (about  $1,400 \pm 190 \text{ kg/m}^3$ ) materials with relative dielectric constants near  $2.7 \pm 0.3$  are present within the uppermost 2 to 3 m. Because the radar waves would be unaffected by a few centimeters of loose dust, the surface materials of Arabia may be chiefly (97%) moderately dense materials overlain by a few centimeters of dust and 0.04 to 0.4 m rocks (3%). The moderately dense materials may be cemented or compacted dusts. Thus, the rate that processes cement and compact dust in Arabia may, in fact, be comparable to the rate that loose dust accumulates (19).

Analyses of both the polarized and depolarized echoes from continuous wave radio transmissions at 12.5-cm wavelength are in progress and additional observations will be made this year. These observations and analyses will provide important information on the distributions, thicknesses, and nature of dusts on Mars.

#### References

1. Harmon, J.K., and Ostro, S. J., 1985, Icarus, 62, 110-128.
2. Harmon, J.K., Ostro, S.J., and Campbell, D.B., 1982, Icarus, 52, 171-187.
3. Thompson, T.W., 1987, LPS XVIII, 3, 1018-1019.
4. Thompson, T.W., and Moore, H. J., 1988, LPS XIX, 3, 1199-1200.
5. Thompson, T.W., and Moore, H. J., submitted, LPSC XIX, 49 p.
6. Scott, D.H., and Tanaka, K. L., 1986, U.S.G.S. Misc. Inv. Map I-1820-A.
7. Greeley, R., and Guest, J.E., in press, U.S.G.S. Misc. Inv. Map.
8. Moore, H.J., unpublished maps.
9. Palluconi, F.D., and Kieffer, H.H., 1981, Icarus, 45, 415-426.
10. Christensen, P.R., 1986a, J.G.R., 91, 3533-3545.
11. Christensen, P.R., 1986b, Icarus, 68, p. 217-238.
12. Hagfors, T., 1967, Radio Sci., 2, p. 445-465.
13. Thompson, T.W., and Dyce, R.B., 1966, J.G.R., 71, 4843-4853.
14. Evans, J.V., and Hagfors, T., 1964, Icarus, 3, 131-160.
15. Jakosky, B.M., 1986, Icarus, 66, 117-124.
16. Campbell, M.J., and Ulrichs, J., 1969, J.G.R., 74, 5867-5881.
17. Moore, H.J., and Jakosky, B.M., submitted to Icarus, 39 p.
18. VonHippel, A.R., 1954, John Wiley and Sons, 430 p.
19. Christensen, P.R., 1982, J.G.R., 87, 9985-9998.

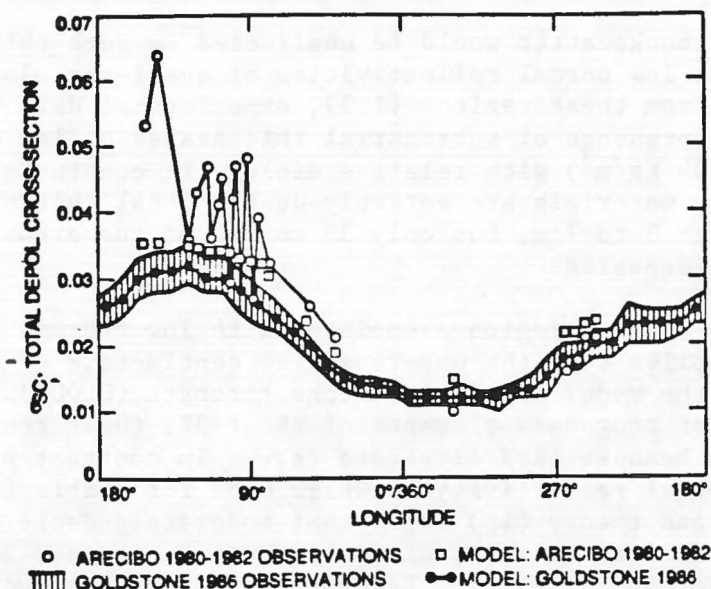


Figure 1. Model and observed total radar cross sections for depolarized echoes as a function of longitude. Goldstone cross sections are averages in 10° longitude bins between 3° and 14° S. Arcicibo cross sections are single observations between 22° and 25° N. Model cross sections are at 7°S and the same latitudes as the observations in the north.

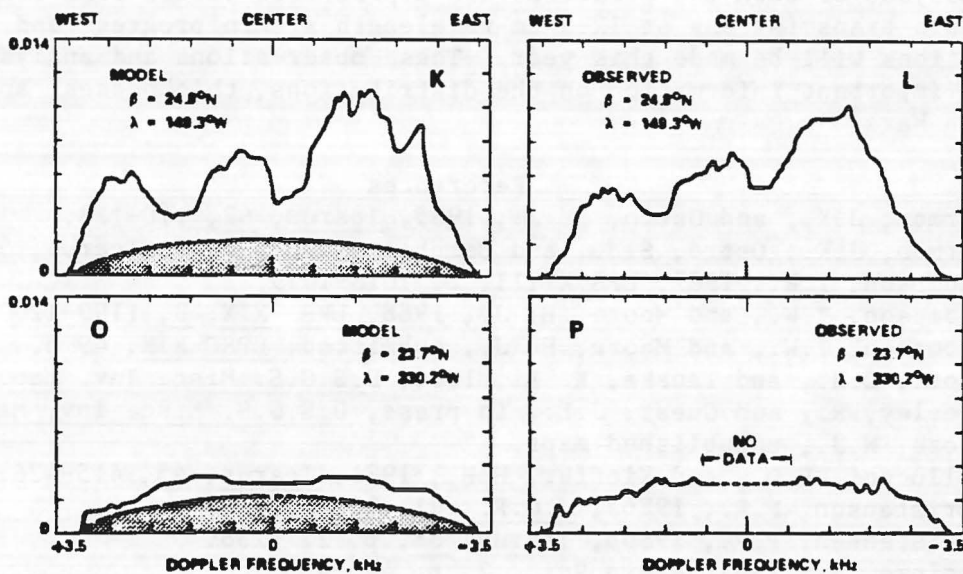


Figure 2. Model and observed depolarized echo spectra for two Arcicibo observations at the indicated latitudes and longitudes. Note that the model and observed spectra are similar. The double hatched area shows the model spectrum for a featureless, uniformly bright planet with a total cross section of 0.010. K and L represent spectra dominated by lava plains and volcanoes. O and P represent spectra dominated by cratered uplands and Arabia.

MARS GLOBAL ATMOSPHERIC OSCILLATIONS: ANNUALLY SYNCHRONIZED, TRANSIENT NORMAL MODE OSCILLATIONS AND THE TRIGGERING OF GLOBAL DUST STORMS; J. E. Tillman, Department of Atmospheric Sciences, AK-40, University of Washington, Seattle, Wa., 98195

Observation and analyses of the atmospheric pressure at the surface on Mars for several Martian years, has revealed transient events in the daily pressure variations which may be Kelvin normal mode oscillations and these or similar oscillations may be a necessary ingredient in the initiation of Martian global dust storms. The transient events last only a few sols, ( Mars days ), appear to repeat on an annual basis to within a few sols, appear to cover a large portion of the hemisphere on the same sol or at least within a few sols, occur in pairs with separations of 20 sols ( in some instances ), and are coincident with the annual pressure minimum, ( i.e., the maximum concentration of carbon dioxide in the southern hemisphere ). Prior analyses of these transient pressure oscillations suggested that they differed from exact harmonics of the diurnal cycle but did not have adequate spectral resolution to make any definitive conclusion. A reanalysis of the data with higher resolution shows that they consist of spectral components generally near to and sometimes identical in frequency with the diurnal and semi-diurnal harmonics. It is suggested that these events are transient, Kelvin, normal mode, global oscillations due to their close agreement in frequency with theoretical calculations. Simulation of composite diurnal and almost diurnal harmonics and analyses with the same techniques and parameters demonstrates that the two nearby, but distinct, spectral lines apparently are not artifacts of the analytical techniques. Comparison of the frequencies with theoretical calculations of Hamilton and Garcia [1], 1984 and Zurek, (private communication 1988), suggests that these are Kelvin, wavenumber 1 and 2 modes which are symmetric with respect to the equator.

Examination of the initiation of the 1977 A, 1977 B and 1982 A global dust storms indicate that pseudo-diurnal harmonic oscillations might be involved in triggering the global dust storms, possibly in conjunction with winds due to baroclinic and Hadley circulations. Prior to the 1977 B global dust storm, the diurnal harmonic disappears and is replaced by an oscillation at 1.1 cycles/sol. If the lack of a classical diurnal tide indicates the suppression of convection, this might partially explain the slow growth of the 1977 B storm. The daily average pressure during the transient season, which precedes the global dust storm season by almost 1/4 of a year, exhibits a different behavior during the global dust storm years than during non global dust storm years. This implies that the global circulation must differ significantly in these cases and may be related to the presence or absence of global dust storms later in a given year.

Wind data will be discussed in the context of changes during the transient events to assess their support for the Kelvin mode hypothesis. In general, these analyses suggest that normal mode, high frequency global oscillations, different from the classical solar driven tides, may be quite common on Mars and may be necessary for the initiation of the global dust storms.

## References

- [1] Hamilton, K. and R. R. Garcia, Theory and Observations of the Short-Period Normal Mode Oscillations of the Atmosphere. *J. Geophys. Res.*, 91, D11, 867-875, 1986.

MARTIAN GREAT DUST STORMS: APERIODIC PHENOMENA? R. W. Zurek, Jet Propulsion Laboratory, California Institute of Technology, Pasadena, CA 91109, and R. M. Haberle, NASA Ames Research Center, Moffett Field, CA 94035

The frequency of occurrence of martian great dust storms accounts for much of the interannual variability of the atmospheric thermal structure and circulation on Mars. These storms profoundly affect the seasonal climatic cycles in any year in which they occur. On very long (i.e., astronomical) time scales, the great dust storms may provide the dust which appears in the polar laminated terrain and in long-term dust deposits elsewhere on the planet.

On all these time scales, from seasonal to interannual to very-long-term, the frequency with which dust storms occur is critical to quantifying their climatic effects. There are two limiting scenarios for this frequency of great dust storm occurrence: (1) the great dust storms occur nearly every martian year, in response to a seasonally occurring "trigger," or (2) the great dust storms are not periodic, or even quasi-periodic, at all, but rather occur as part of a highly nonlinear, stochastically forced system.

Zurek (1982) argued that, based on the Viking Lander surface pressure data and on both Earth-based and spacecraft data since 1956, a great dust storm (defined as one which is of planetary scale, though it certainly need not be planet-wide or even planet-encircling) could have occurred nearly every Mars year. Furthermore, it was argued that this scenario was consistent with Earth-based observations earlier in this century, given the natural limitations of viewing Mars from Earth.

Martin (1984) countered by pointing out that relatively few planet-encircling dust storms had ever been viewed on Mars and that these had all occurred since 1955. In particular, he argued that the absence of great dust storms during earlier periods was due to a real lack of storms and not to viewing limitations.

Leovy et al. (1986) noted the two very different northern winter weather regimes that occurred even during the Viking years, depending on whether or not a planet-encircling dust storm occurred that year. They speculated that the occurrence of the storms themselves might be an example of a bifurcation phenomenon whose alternate paths are determined by randomly occurring natural variations in the atmosphere-dust-polar cap system during earlier seasons. On the other hand, Haberle (1986) suggested that the occurrence of the great dust storms was somewhat deterministic, in that the occurrence of a great dust storm one year might suppress the generation of such a storm the following year.

Dust accumulation in surface sinks over time would be very different under these different scenarios for the frequency of the great storms. The present "dusty period" of frequent great dust storms may be quite anomalous. If so, the amount of dust carried into the polar regions during long-term cycles could be much less than that estimated previously from the annual dust cycles observed in the last few decades (e.g., Pollack et al., 1979).

After a brief review of current hypotheses for dust-storm generation and the frequency of that generation, we investigate a model for dust-storm occurrence that would yield a highly aperiodic time series. Following Leovy et al. (1986), we envision that there are two quasi-stable climatic states for Mars, corresponding to years with and without great dust storms, and that the Mars climate system jumps between these two states due to randomly occurring natural perturbations. However, we hypothesize that this transition is asymmetric--that is, Mars may spend more time in the non-dust-storm regime, than in the dusty regime--because of nonlinearities in the physical system. For Mars, the nonlinear feedback may be provided by the radiative-dynamic effects of airborne dust hazes.

The specific model is motivated by a terrestrial model (Vallis, 1986) in which El Niño-Southern Oscillation climatic fluctuations are simulated as a chaotic dynamical system. These terrestrial phenomena resemble the great dust storms on Mars to the degree that both may be aperiodic episodes which have a preferred season for onset and that the strength of the response (as measured by sea-surface temperatures on Earth or visible opacity on Mars) may be quite varied, as will be the global climatic effects.

#### References:

- Haberle, R. M., 1986: Interannual variability of global dust storms on Mars. Science 234, 459-461.
- Leovy, C. B., et al., 1986: Interannual variability of Martian weather. Dynamics of Planetary Atmospheres, G. E. Hunt, ed., Cambridge Univ. Press, pp. 69-84.
- Martin, L., 1984: Clearing the Martian air: The troubled history of dust storms. Icarus 57, 317-321.
- Pollack, J. B., et al., 1979: Properties and effects of dust particles suspended in the Martian atmosphere. J. Geophys. Res. 84, 2929-2945.
- Vallis, G. K., 1986: El Niño: A chaotic dynamical system? Science 232, 243-245.
- Zurek, R. W., 1982: Martian great dust storms: An update. Icarus 50, 288-310.